Information content of space-borne hyperspectral infrared observations with respect to mineral dust properties

L. Klüser[1], J. R. Banks[2], D. Martynenko[1], C. Bergemann[1], H.E. Brindley[2], T. Holzer-Popp[1]

[1] German Aerospace Center (DLR), German Remote Sensing Datacenter (DFD), Wessling, Germany

[2] Imperial College, Space and Atmospheric Physics Group, London, UK

Keywords: mineral dust; infrared remote sensing; IASI; Fennec; information content

Abstract

In principle, observations from hyperspectral infrared (IR) sounders such as IASI (Infrared Atmospheric Sounding Interferometer) can be used to simultaneously retrieve dust aerosol optical depth (AOD) and properties such as dust particle size, composition, emission temperature and height. Starting from a compilation of "typical" mineral dust particle size distributions and mineralogical compositions, the information content of dust spectra from Mie simulations and from FTIR (Fourier-Transform-InfraRed spectrometer) measurements (provided by the University of Iowa) is analysed. While the Mie spectra provide a higher number of degrees of freedom for signal (up to 6.7) than the FTIR spectra (up to 5.7), the Shannon information content is slightly lower (3.4) from Mie than from FTIR (3.5). The analysis shows that the spectra provide information on particle size and composition, but information about both cannot be extracted independently owing to the correlations between the different spectra. A dust retrieval approach for IASI probing the spectral shape of extinction has been updated using the Mie and FTIR spectra. Dust properties provided by the retrieval algorithm are: AOD (at 0.55µm and 10µm), effective radius, mass-weighted mean diameter, weight-fractions of mineralogical components, IR single scattering albedo and dust

layer effective emission temperature. The retrieval uncertainty in each of these parameters is calculated for each IASI pixel. From the retrieved dust layer temperature the dust layer altitude is also inferred using temperature profiles from the WRF numerical weather prediction model.

To evaluate the impact of using Mie and FTIR spectra within the algorithm, AODs determined using each are compared to AERONET and SEVIRI dust observations. This evaluation suggests that the overall performance of the retrieval in terms of AOD is better for the FTIR version. Evaluation (of the FTIR version) with AERONET coarse mode AOD shows a correlation of 0.73 with RMSD of 0.18 and bias of -0.07. 85% of IASI AOD retrievals are found to be within ±0.2 of AERONET coarse AOD. Evaluating the quality of the other retrieved parameters is more difficult, but we find that the values obtained do show a strong dependence on whether the Mie or FTIR spectra are used. For example, using FTIR spectra results in higher spatial variability in the clay fraction of the retrieved dust compared to Mie. Similar sensitivity is seen in the retrieved particle sizes and single scattering albedo. Indeed, assumptions made concerning the absorption properties of the Mie spectra result in the retrieval of unrealistically low dust layer altitudes, while reasonable values are obtained when using FTIR spectra. Thus it is important to acknowledge that good AOD agreement with independent validation sources does not automatically imply a similar level of quality in the remaining variables.

1 Introduction

Mineral dust in the atmosphere has gained increased interest in the scientific community during recent years owing to its important role in the climate system and its impacts on air quality. Airborne dust interacts directly with solar and terrestrial radiation (e.g. *Sokolik and Toon*, 1999; *Slingo et al.*, 2006); dust particles can also act as ice cloud nuclei, altering cirrus microphysical properties (e.g. *De Mott et al.*, 2003). Both direct and indirect effects alter the radiation balance, and thus atmospheric and surface heating. They depend on the microphysical, optical and chemical properties of the dust (e.g. *Balkanski et al.*, 2007; *McConnell et al.*, 2008; *Johnson and Osborne*, 2011). Dust induced perturbations to atmospheric stability can alter atmospheric dynamics, further influencing cloud formation and precipitation (e.g. *Zhao et al.*, 2011).

Dust from the Sahara, the largest dust source in the world (e.g. *Washington et al.*, 2003), acts as an important source of iron for maritime biogeochemistry (e.g. *Mahowald et al.*, 2005) and fertilisation in South America (e.g. *Koren et al.*, 2006). Moreover, desert dust affects regional air quality, also far away from sources, in terms of particulate matter, visibility and even transport of bacteria (e.g. *Prospero*, 1999). Planning and forecasting of solar energy resources, especially in subtropical and arid regions, requires good knowledge about aerosol due to the low cloudiness of the respective regions. In deserts or semi-deserts dust is the major contributor to the atmospheric aerosol load. Knowledge about the atmospheric dust load and its microphysical properties from remote sensing is thus of very high importance for the solar energy sector (*Schroedter-Homscheidt et al.*, 2013). Consequently there is a strong need for satellite observations of the spatio-temporal distribution of mineral dust in the atmosphere.

Owing to Si-O resonance peaks of silicate minerals in the terrestrial infrared (TIR) (e.g. *Kleinman and Spitzer*, 1962), narrow-band satellite observations in this spectral region can be used for dust remote sensing (e.g. *Shenk and Curran*, 1974; *Ackerman*, 1997; *Legrand et al.*, 2001). More recently, algorithms seeking to exploit the higher spectral resolution available from TIR sounders for inferring additional information about dust properties or height have also been developed (e.g. *Pierangelo et al.*, 2004; *DeSouza-Machado et al.*, 2010; *Klüser et al.*, 2011; *Clarisse et al.*, 2013).

Most methods for hyperspectral TIR remote sensing of mineral dust rely on imperfect knowledge about surface emissivity. Consequently, up to now, most of these algorithms are only applied over ocean (e.g. *Pierangelo et al.*, 2004; *DeSouza-Machado et al.*, 2010). In *Klüser et al.* (2011) a method for dust retrieval from IASI (Infrared Atmospheric Sounding Interferometer) observations was described which decomposes the IASI spectrum into singular vectors in order to minimise the impact of surface emissivity and atmospheric state. After initially using dust optical properties from the *Optical Properties of Aerosols and Clouds* (OPAC) package (*Hess et al.*, 1998), the approach was updated to use laboratory-measured extinction spectra of dust by FTIR (Fourier-Transform-InfraRed spectrometer) (*Klüser et al.,* 2012). An evaluation with observations from the Fennec campaign in Northern Africa (Washington et al., 2012) showed a generally good performance, but also some limitations of the method, especially with respect to surface emissivity and dust characterisation (*Banks et al.,* 2013). As a result a detailed examination of the information about dust properties contained in IASI signals and the retrieval approach has been performed and is presented here. The new insights are used to further improve the retrieval method. In particular, Mie and FTIR spectra are used as input to the retrieval algorithm in order to evaluate which is better for characterising airborne Aeolian dust.

In section two the current knowledge about the mineralogical, microphysical and optical properties of airborne dust is reviewed, as this information will be of high importance throughout the remainder of the analysis. In section three an analysis of the information content of dust extinction spectra with respect to dust properties is performed. Section four reviews the fundamentals of the retrieval method and describes its updates and new approaches. In section five retrieval results are presented and evaluated using different metrics and methods, with a focus on evaluating differences obtained when using Mie or FTIR spectra. The discussion in section six is followed by concluding remarks in section seven.

2 Microphysical, mineralogical and optical properties of desert dust

Aeolian dust is characterised by a very high variability in particle sizes (e.g. *Haywood et al.*, 2011; *Johnson and Osborne*, 2011; *Ryder et al.*, 2013), particle shape (*Dubovik et al.*, 2006; *Kandler et al.*, 2007; *Alexander et al.*, 2013), mineralogical composition (e.g. *Glaccum and Prospero*, 1980; *Kandler et al.*, 2007; *Jeong*, 2008; *Engelbrecht et al.*, 2009) and consequently optical properties (e.g. *Sokolik and Toon*, 1999; *Haywood et al.*, 2011; *Alexander et al.*, 2013). While the assumption of spherical dust particles has been suggested to be a suitable approximation for thermal infrared dust retrievals (Yang et al., 2007), there are other studies (including the work of *Hudson et al.*, 2008a;b; *Mogili et al.*, 2008) which indicate that Mie theory causes large uncertainties in the characterisation of highly resolved spectral infrared extinction. In this study retrieval results using the spherical assumption will be compared to results when the retrieval is run with a more realistic characterisation of dust extinction. Particle size and dust composition have been reported to be critical parameters for the setup of any retrieval algorithm (e.g. *Sokolik and Toon*, 1999; *Highwood et al.*, 2003) and so the effects of these parameters are also carefully considered here.

Recently much effort has been spent on characterising aerosol particle size distributions with specific focus on desert dust. Table 1 lists key characteristics of eight particle size distributions for mineral dust, including the number of lognormal modes and mass-weighted mean diameter D_w of the size distributions. These range from the traditional size distribution for transported mineral dust (MITR) of the OPAC database (*Hess et al.*, 1998) and the mono-modal size distribution used in the Aerosol_cci project of the European Space Agency's Climate Change Initiative (*De Leeuw et al.*, 2013) to four-modal representations of particle size distributions sampled during aircraft campaigns. The campaign data show a very high variability in particle size. During the Dust Outflow and Deposition to the Ocean (DODO) experiment (*McConnell et al.*, 2008) only accumulation mode particles with radius smaller than 1.5µm were collected while *Ryder et al.* (2013) report the abundance of very large particles in dust samples during the Fennec campaign over North Africa. Another size distribution reported by *Osborne et al.* (2008) for the Dust And Biomass-burning EXperiment (DABEX) is represented by five lognormal modes. The authors also present a "generic distribution" constructed using two lognormal modes, which is the one referred to here as the DABEX size distribution. The eight size distributions mentioned here are presented in Figure 1. The DODO distributions are restricted to particles with R<1.5µm (*McConnell et al.*, 2008) and the maximum radius for the MITR distribution is 5µm (*Hess et al.*, 1998).

Besides particle size the mineral composition of desert dust is the major source of uncertainty in deriving thermal IR optical properties (*Sokolik and Toon*, 1999; *Highwood et al.*, 2003). Aeolian dust is mainly composed of quartz, clays (such as illite, kaolinite and montmorillonite), carbonates (mainly calcite and dolomite), feldspars (e.g. bytownite, orthoclase and albite) and salts (such as gypsum or halite). Many other components can occur in traces or can provide major contributions to dust composition on local scales (e.g. *Sokolik and Toon*, 1999; *Kahlaf et al.*, 1985; *Kandler et al.*, 2007). The relative abundances of the major components vary strongly regionally (e.g. *Sokolik and Toon*, 1999; *Caquineau et al.*, 2002).

Table 3 provides a compilation of dust composition analyses from different parts of the world based on the references listed in Table 2. For the purposes of this study we choose to characterise the composition in terms of the eight major components listed in the table. For the sake of clarity, the percentages in Table 3 have been normalised such that they sum to 100 %. This means that the contribution from, for example, iron oxides has been neglected throughout this study. While in most cases the residual contribution from minerals not included here is rather small, it can be significant for particular locations, reaching up to 22% and 10 % for the Chinese and Kuwaiti mixtures respectively. For each component the source of the refractive index used in this study for calculating the respective optical properties is provided. The dust mixtures cover the major dust sources of the northern hemisphere as well as deposition regions.

The relative abundance (percentage by weight) of quartz, illite, muscovite, kaolinite, montmorillonite, chlorite, gypsum, calcite (including the dolomite abundance, since the spectra are almost identical) and feldspars is presented for the eight representative mixtures in Table 3. Illite and muscovite are compiled in one group as not all authors separate between these micas (e.g. *Glaccum and Prospero*, 1980). A constant ratio of 1:1:1 for K-feldspar, albite (Na-rich plagioclase) and anorthite/bytownite (Ca-rich plagioclase) is assumed here due to a lack of information about feldspar composition in most studies. That means that the optical properties for feldspars have been calculated for each feldspar component and the equally weighted average has been determined. This average, representing the optical properties of the feldspars, has then been used with the compositional percentage of feldspars listed in Table 3. For the Ca-rich plagioclase the refractive index of bytownite has been used (see Table 2).

To generate Mie optical properties the refractive indices for each of the eight mineral components listed in Table 3 are used together with each of the 8 size distributions given in Table 1 as input to the Mie code described in *Quenzel and Müller* (1987). In this way 64 spectra of extinction coefficient, single scattering albedo (ω_o) and asymmetry parameter (g) are produced, one for each component for each size distribution. In the case of birefringent minerals (quartz and calcite) a ratio of 2:1 for the ordinary and extraordinary rays is used (e.g. *Spitzer and Kleinman*, 1961) for averaging the optical constants before the calculation of the optical properties. Although *Hudson et al.* (2008a,b) found that Mie theory is not able to represent dust particle absorption in the Rayleigh limit ($2\pi r/\lambda << 1$) well, the size distributions reported in Table 1 suggest that large particles outside the Rayleigh regime significantly contribute to the airborne dust and thus that Mie scattering becomes important.

The single component optical properties for each size distribution are then averaged according to the weighting given in Table 3. This again results in 64 spectra, but this time representative of each dust mixture for each size distribution. These spectra of extinction coefficient, ω_0 and g are used in the retrieval following the methodology outlined in section 3. Figure 2 shows ω_0 and g for four out of the eight dust mixtures for the DODO (small particles) and Fennec (large particles) size distributions calculated using Mie theory.

The asymmetry parameter *g* is much lower for DODO than for Fennec spectra for all mixtures which could be expected given the average particle size and the use of Mie theory. Differences between mixtures for the same size distribution are much smaller although for the DODO case there is a distinct change in shape for the Central Saharan mixture. As will be evident from the simulation of dusty spectra in section 3, the spectral shape of the asymmetry parameter impacts on the shape of the effective extinction spectra as seen from space (see e.g. *Ackerman*, 1997).

The single scattering albedo for the Fennec size distribution is typically higher than for the DODO size distribution, particularly at the bottom and top of the wavenumber range considered here, but the impact of changes in composition for this size distribution is relatively small. Composition appears to have more of an impact for the DODO size distribution, with a very marked change in single scattering albedo for the central Saharan mixture, both in shape and magnitude. The Central Saharan dust mixture is significantly more absorbing than the other mixtures for small particles (DODO size distribution). Similar behaviour is not seen for the Fennec distribution. In fact for the other mixtures shown here single scattering albedo is comparable between the Fennec and DODO size distributions, although the FENNEC size distribution includes much larger particles. The single scattering albedo spectra indicate that scattering contributes significantly to the dust extinction, and this is also true of spectra from the DODO size distribution. From these results it is not clear whether the high scattering signal for small particles is the result of the mineralogical composition (where the Central Sahara with the minor quartz contribution would be an exception) or if the use of Mie calculations assuming spherical particles yields unreliable single scattering albedo depending on the composition (as a result of the refractive indices).

The FTIR spectra analysed in *Hudson et al.* (2008a;b) and in *Mogili et al.* (2008) were measured at the University of Iowa as described in the publications referred to above. The extinction data together with the size distributions characterising the samples have been obtained by personal communication from the University of Iowa (P. Kleiber and V. Grassian). As the FTIR spectra do not provide ω_0 and g, these have been treated differently as will be outlined in section 3. Note that the solutions proposed by *Hudson et al.* (2008a;b) and *Mogili et al.* (2008) do not provide ω_0 and g and consequently are not well suited for use in this study.

The selection of dust refractive indices would be expected to strongly influence the retrieval results (e.g. *Brindley and Russell, 2006; Pavolonis et al.,* 2013). This impact is manifested more clearly as spectral resolution is increased from narrowband to hyperspectral information and when dust mineralogical composition is varied. While for almost all mineralogical components typically found in Aeolian dust in significant contributions (see Table 3) there are TIR optical constants described in the literature (Table 2), the resulting refractive indices for one mineral presented by different authors can show significant disagreement. For example quartz extinction spectra simulated with Mie theory for the GERBILS size distribution using refractive indices from six different authors are presented on the right side of Figure 1. The refractive indices used are from *Peterson and Weinman* (1969), *Wenrich and Christensen* (1996), *Longtin et al.* (1988), *Russell and Bell* (1967), *Spitzer and Kleinman* (1961), *Steyer et al.* (1974) and *Koike et al.* (1989). An average is also provided, which has been calculated by averaging the optical constants before running the Mie code. The vertical dashed lines bound the strong ozone absorption band in the terrestrial window, which is not used for dust retrieval (*Klüser et al.*, 2001; 2012). The *Russell and Bell* curve is almost identical to that from *Spitzer and Kleinman* (as noted by *Russell and Bell*, 1967) and at the spectral resolution considered here (10 cm^{-1}) cannot be distinguished in the curves in the Figure. It is evident that using one set of refractive indices or another will produce very different results when the spectral behavior of quartz extinction in the TIR is important (i.e. when single IASI channels are used or when the spectral shape of dust extinction spectra is compared to observations). For the case of quartz and the retrieval method used throughout this study, the selection of refractive indices cause an uncertainty in AOD of up to 22.4% for the quartz component. A similar uncertainty can apply for other minerals (~15% for clays) although the issue is less marked for components such as carbonates and gypsum (uncertainty ~2-3%). Due to the lack of a significant number of measurements of refractive indices for feldspars (see e.g. *Lee and Park*, 2014) the uncertainties brought about by the selection of refractive index data for this class of minerals remains unknown.

The black and red dashed curves in Figure 1 represent FTIR measurements of quartz samples with two different size distributions and are shown for comparison. FTIR sample #1 represents dust in the Rayleigh limit as described in *Hudson et al.* (2008a). Sample #2 represents dust particles with a broader size distribution (*Mogili et al.,* 2008). It includes a larger contribution of scattering by the dust particles to the dust extinction (increased single scattering albedo). It can easily be seen that all Mie spectra show a blue shift of the extinction peak compared to the FTIR measurements as noted by *Hudson et al.* (2008a) and *Mogili et al.* (2008). At our spectral resolution of 10cm^{-1}, the blue shift of the extinction peak ranges from 10cm^{-1} (for the *Koike et al.* refractive indices) to 50cm^{-1} (for the *Peterson and Weinman* and the *Longtin et al.* refractive indices). *Hudson et al.* (2008a) found a blue shift of 55cm^{-1}, *Mogili et al.* (2008) one of 58cm^{-1}. Given the coarser spectral resolution used here the blue shift values of Hudson *et al*. as well as of Mogili *et al*. can be considered comparable to the range of results we obtain, especially when using the refractive indices of *Peterson and Weinman* (1969) or *Longtin et al.* (1988).

In the remainder of this study the pre-tabulated refractive indices from *Peterson and Weinman* (1969) have been used for all Mie simulations for quartz. As can be seen from Figure 1, none of the Mie spectra are able to provide a good approximation to the measured FTIR extinction spectra (see also *Hudson et al.*, 2008a; *Mogili et al.*, 2008). Nevertheless we assume that the distinct blue shift in the spectra could also be a result of particle nonsphericity and treatment of absorption in the Mie calculations.

Although other aerosol types are present episodically in regions of frequent dust occurrence these do not contribute substantially to the IR extinction spectra since the aerosol extinction efficiency in the presence of aeolian dust is dominated by the Si-O absorption resonance of silicates. Other aerosols, such as those arising from combustion, contribute mainly to the fine mode and consequently fall into the Rayleigh regime, where scattering effects in the TIR are small (e.g. *Klüser et al.*, 2011; 2012).

3 Information content of dust spectra

In *Klüser et al.* (2011) and *Klüser et al.* (2012) a method for retrieving visible dust AOD from IASI observations was developed. The aim of this section is to analyse the information content of the IASI spectra with respect to dust properties, i.e. to show which information is carried in the signal and can be extracted by the retrieval. Therefore, first the pure dust signal neglecting all atmospheric effects and surface emissivity is analysed, and then the approach is applied to real IASI observations in the next step.

In order to avoid contamination by narrow gas absorption lines while still using much of the available spectral information contained in IASI measurements the observations are collected into bins, of 10 IASI channels each and the observations with highest brightness temperatures are assumed to be least affected by the atmospheric state (*Klüser et al.*, 2011). From 420 channels between 833cm^{-1} and 1250cm^{-1} 42 spectral bins are derived. Among those, seven bins are highly contaminated by strong O_3 absorption and are not used, resulting in 35 spectral bins used in the dust retrievals (*Klüser et al.*, 2012).

In previous versions of the retrieval algorithm the impact of scattering and thermal emission on the spectral shape of the dust signal was neglected (*Klüser et al.*, 2011; *Klüser et al.*, 2012). Nevertheless *Ackerman* (1997) shows the impact of both on the spectral behavior of aerosol extinction as well as on the sensitivity of satellite observations to aerosol loading. As a consequence the Two-Stream approach suggested by *Ackerman* (1997) for radiative transfer in a dusty atmosphere has been applied here. Although the Two-Stream solution strongly simplifies the radiative transfer problem it is assumed that multiple scattering between aerosol layers may be neglected under most naturally occurring conditions (*Ackerman*, 1997). Hence this method is assumed to be sufficient for accounting for the impact of scattering and thermal emission of the dust on the spectral shape of the extinction. In the case of purely absorbing aerosol the Two-Stream solution simplifies to the approach used in previous retrieval versions. The Two-Stream approach in the form described in *Ackerman* (1997) totally neglects surface emissivity as well as absorption and emission of the atmosphere itself. Such an approximation can be called “black surface – transparent atmosphere” (BSTA approximation) and guarantees that the information content to be analysed in the following section really is from differences in dust spectra and not from differing atmospheric profiles.

If the aerosol layer is not opaque, the effective transmittance of a dusty atmosphere according to *Ackerman* (1997) depends on the temperature of the dust (T_{dust}) as well as its optical properties. It is defined as the ratio of observed radiance I_{obs} to surface leaving radiance $I_{\uparrow}$ and is given by

$$\frac{I_{obs}}{I_{\uparrow}} = \frac{1}{2}\left[\frac{e^{-k\tau}+\frac{M_+}{M_-}}{\frac{M_+}{M_-}e^{-k\tau}+1}+\frac{\frac{M_+}{M_-}-e^{-k\tau}}{\frac{M_+}{M_-}e^{-k\tau}+1}\right]+\frac{I_{\downarrow}}{2I_{\uparrow}}\left[\frac{e^{-k\tau}+\frac{M_+}{M_-}}{\frac{M_+}{M_-}e^{-k\tau}+1}+\frac{\frac{M_+}{M_-}+e^{-k\tau}}{\frac{M_+}{M_-}e^{-k\tau}+1}\right]+\frac{B(T_{dust})}{I_{\uparrow}}\left[1-e^{-k\tau}\right] \tag{1}$$

with

$$k = \sqrt{(1-\omega_0)(1-\omega_0 g)} \tag{2}$$

$$M_{\pm} = \frac{1}{1 \pm k}\left(\omega_0 \mp \omega_0 g (1-\omega_0)\frac{1}{k}\right) \tag{3}$$

where $I_{\downarrow}$ is the downwelling radiance from above the dust layer. In accordance with the methodology proposed in *Klüser et al.* (2011) and *Klüser et al.* (2012) equivalent optical depth (τ_{eqv}) is used instead of effective transmittance. The former can easily be derived from the latter by

$$\tau_{eqv} = -\ln\left(\frac{I_{obs}}{I_{\uparrow}}\right) \tag{4}$$

Figure 3 shows optical depth spectra calculated with Equation (1) for all eight dust mixtures presented in Table 3. The AOD spectra are normalised to the averaged value from 925cm^{-1} (Al-O-H peak, e.g. from kaolinite) and 1125cm^{-1} (Si-O peak). This averaged AOD value will be referred to as AOD_{IR} in the remainder of the text. All spectra in Fig. 3 have been calculated with $T_{surface}$ = 290K, T_{dust} = 270K and the BSTA approximation. The spectra in the top row are derived from Mie simulations of optical properties for the dust particle size distributions of the DODO and Fennec campaigns.

The bottom row shows the spectra obtained from FTIR size modes #1 (*Hudson et al.*, 2008a; *Hudson et al.*, 2008b) and #2 (*Mogili et al.*, 2008) with significantly differing size distributions (see Figure 1). The extinction spectra in the two different size modes are provided for the different components separately. Nevertheless some components were measured only in one size mode. For example anhydrite extinction was not measured in the size range of mode #1. Mie simulations suggest that for anhydrite the impact of the size distribution on the spectral shape of the extinction is rather small, consequently the anhydrite extinction spectrum from mode #2 has been scaled with integrated Mie extinction efficiencies to the size range of mode #1 (by averaging the size distributions of the other components). For the size range of mode #2 no feldspar measurements were made. Thus feldspar in mode #2 is accounted for in an analogous manner to anhydrite in mode #1.

In order to obtain the single scattering albedo and asymmetry parameter (required by the Two-Stream approximation) from the FTIR extinction measurements, we assume that mode #1 is in the Rayleigh limit, i.e. is almost purely absorbing (see *Hudson et al.*, 2008a,b). If one assumes that the spectral shape of the absorption signal varies only very slightly with particle size and that the broadening of the extinction peak is mainly the result of scattering (*Salisbury and Wald*, 1992), the spectrally varying factor k in Equation (1) can be estimated as the ratio between the normalised extinction of mode #2 and mode #1 for each component separately. In addition, to correctly treat the contribution of different components to TIR extinction in the spectra of dust mixtures, the extinction over the total spectral range has been integrated from Mie simulations performed with the respective size distributions of the samples. This spectrally integrated extinction has been used to scale the FTIR spectra with respect to extinction coefficients before mixing. Normalisation has then only been applied to the spectra of the dust mixtures (in contrast to the approach followed in *Klüser et al.*, 2012, where FTIR spectra of the separate components were normalised and were then used in the retrieval).

While eight size distributions have been used for Mie spectra, as noted previously, FTIR spectra are only available in two size classes: very small particles in the Rayleigh limit in mode #1 and larger particles with broader size distributions in mode #2 (see *Hudson et al.*, 2008a,b; *Mogili et al.*, 2008 for details of the size distributions of the FTIR samples). In order to compare retrieval results of the Mie and FTIR versions we intended to use exactly the same retrieval code and just vary the input data. Consequently the FTIR spectral database had to be expanded to eight size modes. This has been done by equidistant interpolation between the two measured modes (#1 and #2) to an eight-mode FTIR database.

Furthermore, equivalent optical depth spectra using the BSTA approximation have been calculated for both sets (Mie and FTIR). Again, surface temperature has been kept constant at 290K while dust temperature has now been varied between 220K, 230K, 240K, 250K, 260K, 270K, 280K and 285K. Together with eight AOD values (varying between 0.01 and 1.0) eight mixtures and eight size distributions this gives a total of 4096 spectra for each set for analysing the information content.

The number of independent pieces of information relating to mineral dust properties present in a measurement can be obtained by applying the concept of degrees of freedom for signal (*Rodgers*, 2000) to the simulated or satellite aerosol observations (*Martynenko et al.*, 2011). Given the averaging kernel matrix ***A***=***GK*** with weighting function ***K*** and gain matrix ***G*** (see *Rodgers*, 2000 for details) the degrees of freedom for signal (*DFS*) are calculated as the trace of matrix ***A***:

$$DFS = tr(A) \tag{5}$$

From Figure 4 it can clearly be seen that the number of DFS increases with AOD_{IR} and with the difference between the temperature of the dust layer and the surface. Although it clearly impacts on the spectral shape of the extinction (see Figure 3) particle size does not impact as strongly on *DFS* (not shown). Consequently, increasing or decreasing dust particle size does not yield more or less information about dust properties. This means that for small particles the same amount of information can be retrieved as for large particles, if everything else is kept constant. The results of Figure 4 also imply that for low AOD_{IR} and high dust layer temperatures the extractable information in the spectra nearly vanishes. In other words, information about dust properties beyond AOD_{IR} gets more and more reliable the higher the infrared optical depth of the dust and the higher the contrast between dust layer and surface temperatures is. As the ratio of infrared AOD to visible AOD is a function of particle size and mixture, these results also imply that the inferred visible dust AOD will not be very reliable for thin, low level dust. In total 6.7 (Mie) and 5.8 (FTIR) independent pieces of information are contained in the spectra. The *DFS* clearly approaches this number for high AOD_{IR} and low T_{dust} in both cases, but the *DFS* values decrease more strongly towards low AOD_{IR} and low T_{dust} for the FTIR spectra.

As a second examination, the Shannon information content *H* is used, which gives a scalar quantity, related to the total number of independent (atmospheric) states which can be distinguished from each other with a given measurement technique. It gives a quantitative estimation of the independent information contained in the observations, and thus is complementary to the number of degrees of freedom for signal (*Rodgers*, 1998; 2000). The information content of a signal, H, is expressed as an entropy-like number calculated from the probabilities p_i of independent messages (or, in our case, states i) as (*Shannon and Weaver,* 1949):

$$H = -\sum_i p_i \log_2(p_i) \quad (6)$$

The spectral distribution of information about the dust can be expressed by the information spectrum (*Rodgers*, 1998) representing the information content per spectral bin. Therefore for each bin the probabilities in Equation (6) are estimated by histograms of $\tau_{eqv}(\nu)$, calculated over all spectral information used in this study (i.e. all mixtures, size distributions, optical depths and dust layer temperatures also used in the DFS analysis above). The information spectra of the Mie and FTIR representations of dust are presented in Figure 5. It is evident that the spectral distribution of information is different for the Mie and FTIR spectra. Nevertheless, in both cases the maximum information about the dust is contained in the 1100-1200 cm^{-1} (8-9μm) spectral band. The increased information content at about 875 cm^{-1} can be interpreted as the respective calcite extinction peak (see *Hudson et al.*, 2008a and *Klüser et al.*, 2012). Here the signal carried by the observation strongly increases information about the dust impact on the radiance field and thus about the dust properties.

If one were to assume that the information in each channel is uncorrelated, the information content of the simulated IASI spectra would sum up to about 80. But of course such an assumption is not valid: the extinction information is spectrally highly correlated (see Figure 3). Consequently the total information content of the Mie and FTIR spectra is much lower at 3.42 and 3.53 respectively. These numbers translate to about 11 independent dust states which can be distinguished in the spectra. As this number is much smaller than the number of states the information content was calculated from, the information within the dust spectra may be interpreted as being related to different resonance peaks (Si-O, Al-O-H, Ca-O), i.e. dust chemistry within the eight mineralogical dust mixtures. This again indicates that there is significant correlation between the spectra of different mixtures and particle size distributions. Moreover, information about scattering effects (related to the particle size) and differences in thermal emission (related to dust temperature) is also present.

Over deserts, besides the influence of humidity on infrared retrievals (e.g. *Brindley et al.*, 2012) surface emissivity is also a major constraint (e.g. *Banks et al.*, 2013). These constraints have been totally neglected in the analysis of Figures 4 through 6. The information content of the real IASI observations with respect to airborne Aeolian dust is consequently only a subset of the information content characterised in this section as the dust signal may be partially masked by humidity and surface effects. In the next section it is therefore outlined how the impacts of these factors can be minimised in the IASI retrieval method.

4 Algorithm update for IASI

Reduced resolution IASI radiance spectra (*Klüser et al*., 2011) are converted into "equivalent optical depth" spectra with Equation (4). In contrast to the analysis presented in section 3, viewing geometry is also accounted for in the satellite retrieval. The upwelling radiance $I_\uparrow$ is represented by the Planck-function of a baseline temperature, defined as the maximum observed brightness temperature in the spectrum.

To assess the representation of specific spectral patterns within the observations the 4096 simulated spectra are decomposed into principal components by solving the Eigenvalue problem of the covariance matrix (e.g. *Menke*, 2012). From the total number of degrees of freedom (previous section) it can be concluded that eight modes of variability suffice to represent the spectral signal of airborne dust. Thus the load c_i of each of the leading eight Eigenvectors V_i is determined as outlined in *Klüser et al.* (2011):

$$c_i = \sum_{j=1}^{35} \tau_{eqv}\left(\nu_j\right)\cdot V_i\left(\nu_j\right) \qquad (7)$$

where ν_j represents the wavenumber of spectral bin *j* out of 35 spectral bins (*Klüser et al.*, 2012).

As the spectral patterns of the simulated dust spectra are closely related to the optical properties (extinction, single scattering albedo, asymmetry parameter), the Eigenvectors (V_i) carry information about particle size and dust mixture which determine the optical properties. Consequently, the effective dust particle size and the effective dust mixture are estimated directly from the Eigenvector loads and weighting factors of the simulated spectra corresponding to the respective size distribution and mixture.

The simulated dust spectra also contain the signal of dust layer height represented by the temperature difference between dust and surface as well as by the spectra of single scattering albedo and asymmetry parameter (i.e. the spectrum of *k*, Equation (2)). Consequently, the selection of effective radius and mixture implicitly takes into account the masking impact of thermal emission, i.e. for low level dust layers, where the spectral contrast is highly reduced (*Ackerman*, 1997).

In contrast to previous versions AOD_{IR} is no longer retrieved as the projection of the full simulated dust spectrum on a subset of singular vectors, but by projecting the best fitting dust spectrum to the full observations in the spectral range from 830cm^{-1}-980cm^{-1} (15 spectral bins) where the spectral variability of surface emissivity is still rather low (e.g. *Hulley et al.*, 2009). This approach gives a better account of the spectral signature of the dust extinction. AOD_{IR} is transferred to visible AOD (at 0.55µm) by calculating the transfer function using Mie simulations (*Klüser et al.*, 2012). In the case of the FTIR spectra Mie simulations are also used, owing to the fact that the extinction spectra do not range into the visible.

Although it is well known that particle shape is very important in the visible spectrum (e.g. *Dubovik et al.*, 2006; *Alexander et al.*, 2013; *De Leeuw et al.*, 2013) and for 0.55µm extinction coefficients (used here to calculate visible AOD from infrared observations), Mie calculations across the whole spectrum are used for calculating the AOD_{VIS}/AOD_{IR} ratio for each mixture and size mode for the sake of consistency. In addition, in the compilation of dust composition in Table 3 the content of iron oxides (hematite and goethite) is reported in only one case. Although the impact of iron oxides on the spectral shape of infrared extinction in the atmospheric window is very small (*Sokolik and Toon*, 1999), they strongly contribute to absorption in the visible spectrum (e.g. *Sokolik and Toon*, 1999; *Kandler et al.*, 2007). This variable absorption of solar radiation due to varying iron oxide abundance is currently not accounted for in the TIR method presented in this study. Consequently absorption at visible wavelengths will be underestimated when iron oxide abundance is high. In addition, the FTIR samples do not cover the full range of particle sizes (Figure 1), especially near dust source regions. Consequently smaller particle sizes are retrieved from these samples, impacting on all other retrieved dust properties.

The temperature difference between surface and dust layer is estimated from the eigenvector loads. The surface temperature is not equal to the baseline temperature in the principal component decomposition, especially at higher IR optical depths. Consequently, AOD_{IR} is used to estimate the surface temperature before converting the Eigenvector loads into dust effective emission temperature. The resulting effective dust layer temperature can then be converted into dust layer geometrical height using output of numerical weather prediction (NWP) models. The meteorological simulations were performed using the WRF (Weather Research and Forecast) model with ARW (Advanced Research WRF) core (*Skamarock et al.*, 2008). They are based on forecast results from the Global Forecast

System (GFS). The model is initialised using the 18UTC forecast of the previous day in order to allow for some spin-up. Simulations are performed at a horizontal resolution of 30km. 40 vertical levels extending up to 50hPa are included, providing a vertical resolution ranging from 200-300m within the lower troposphere (~1km height) to around 700-800m in the medium troposphere (~4km height). The simulation domain used here covers north and central Africa as well as the western Atlantic and large parts of Europe. Dust layer height is then inferred from the retrieved dust emission temperature by interpolation of WRF temperature and geopotential height fields.

The methodology outlined above is applied twice within the retrieval method: once with dust spectra and properties as described here and once with ice cloud spectra simulated using the ice cloud optical properties of *Yang et al.* (2005). Consequently, ice cloud properties are also determined by the method. Discrimination between Aeolian dust and ice cloud is performed *a posteriori* based on the retrieval results. The *a posteriori* likelihood P_{dust} of the best matching linear combination of dust (ice) spectra scaled with the retrieved IR optical depth (τ_{sim}) and the true observations (τ_{eqv}) is characterised by the normalised projection of one onto the other (*Klüser et al.*, 2011):

$$P_{dust} = \frac{\sum_j \tau_{eqv}(\nu_j) \cdot \tau_{sim}(\nu_j)}{\sqrt{\sum_j \left(\tau_{eqv}(\nu_j)\right)^2} \cdot \sqrt{\sum_j \left(\tau_{sim}(\nu_j)\right)^2}} \qquad (8)$$

As the normalised projection ranges from 0 to 1 and 1 is a perfect fit (i.e. both vectors are parallel), P_{dust} (or P_{ice}) can be interpreted as the probability that the selected dust (or ice) model represents the observations.

Discrimination between dust and ice clouds is then achieved by simply selecting the retrieval output (dust or ice cloud) with the higher *a posteriori* probability. Note that the selection is only made for cases where the retrieved ice cloud effective emission temperature is lower than 265K, otherwise the ice retrieval is rejected as unphysical and the likelihood of ice cloud is set to 0. Liquid water clouds are not detected with this method, as the spectral contrast is smaller and also as dust over liquid water clouds can be detected (see *Klüser et al.*, 2011).

5 Results: dust properties retrieved from IASI, evaluation and sensitivity of results to the selection of spectra

5.1 Retrieved dust properties

As outlined above, the retrieval algorithm provides infrared AOD (average over the AOD in the 925cm^{-1} and 1125cm^{-1} bins) alongside particle size, mineralogical composition and emission temperature of dust. The dust properties are then used to calculate 0.55μm dust AOD. The associated uncertainty in AOD is estimated for each pixel from the uncertainties resulting from the selection of the dust mixture and size distributions as well as from the *a posteriori* estimation of the surface temperature. The particle size distributions used in the retrieval are described by effective radius as well as mass-weighted mean diameter (see e.g. *Mogili et al.*, 2008), consequently both descriptions of dust particle size are also provided as output. The mineralogical composition is expressed in weight percentage of the respective mineral (eight species form Table 3). IR single scattering albedo (averaged over the same bins as IR AOD) is also retrieved as a result of the combination of particle size distribution and mixture.

Figure 6 shows IASI retrievals of visible and infrared AOD of airborne dust over North Africa and the Arabian Peninsula on June 17th, 2011 using Mie and FTIR dust spectra. It is evident that the selection of the spectral database (FTIR or Mie) has a significant impact on the retrieved AOD. Using FTIR spectra the infrared dust AOD is much lower than the value retrieved using Mie spectra and the spatial distribution of elevated dust AOD looks slightly different between both versions. Owing to the very different transfer functions (resulting from particle size and compositions), the visible AOD does not differ as strongly as the IR AOD between both versions in Figure. 6.

Examples of other retrieved dust properties are shown in Figure 7. Mineralogical composition is expressed in the figure as clay fraction, including the relative contributions of illite, kaolinite and montmorillonite to the retrieval results (the retrieval provides the contribution of all eight components to the dust signal). It is evident that mineralogical composition and particle size show greater spatial variability when Mie spectra are used. The most striking difference between the Mie and FTIR versions can be seen for dust layer altitude. In both cases the effective dust layer emission temperature as retrieved from the Eigenvector signal is converted to altitude using the same WRF temperature profiles and interpolation. For the FTIR version the dust altitude ranges from near surface to about 6km. The strong dust plume over the Western Sahara reaches heights of about 6km, while most of the weaker dust inside the Sahara is concentrated between the surface and about 1-2km. Over the Mediterranean the dust (with rather low optical depth) reaches altitudes of about 2-3km while over the Atlantic Ocean it is transported at about 4-6km (which is the typical altitude of dust transported within the Saharan Air Layer, see *McConnell et al.*, 2008). In the Mie version of the retrieval most of the dust is concentrated very close to the surface. Only in the southern Sahara and over the oceans does the dust reach altitudes of about 2km. If all dust within the lowest 500m were excluded from the analysis only a few dust observations would be apparent. Dust AOD uncertainty is generally found to be around 25-35% with higher values at high AOD, where the contribution of the dust emission is highest.

5.2 Evaluation and sensitivity to the choice of spectra

In order to evaluate both versions of the IASI dust AOD and to analyse the performance of both with the goal of deciding which one might be better suited for studying airborne desert dust properties, independent reliable observations are needed which are capable of separating dust AOD from total AOD. Unfortunately AERONET does not provide “Dust AOD” as a product. For the Fennec comparison (Figures 9 and 10) total AOD from AERONET of a subset of sites has been used for comparison with the Dust AOD retrieved from satellite measurements. In regions such as the Sahel, where contributions of dust and biomass burning aerosol to the total aerosol load change with season, total AOD does not always represent the dust AOD. Following *Dubovik et al.* (2002), AOD is classified as dusty where the Ångström exponent (evaluated at 440nm and 870nm) is lower than 0.6 and 1020nm AOD is larger than 0.2 (as also performed for *Banks et al.*, 2013). At sites downwind of the dust sources in the far-range transport regime (e.g. Caribbean, Japan) this selection becomes problematic, as AOD gets lower (i.e. AOD at 1020nm falls below 0.2) and other aerosols contribute to the total aerosol load, increasing the Ångström exponent. In previous studies coarse mode AOD provided by the AERONET Spectral Deconvolution Algorithm (*O’Neill et al.*, 2003) has been selected as the best representation of dust AOD (*Klüser et al.*, 2011; *Klüser et al.*, 2012).

An analysis of dust retrievals during the Fennec campaign (*Banks et al.*, 2013) revealed that the former version of the IASI retrieval typically failed to capture high visible AODs, especially in regions with low surface emissivity at 8.7µm. A similar analysis to that performed in Banks et al (2013) is now presented with the two versions of the updated IASI retrieval again compared to the SEVIRI dust AOD product.

Figure 9 compares the Mie and FTIR versions of the IASI retrieval with the SEVIRI dust product (*Brindley and Russell*, 2009; *Banks and Brindley*, 2013) and AERONET (Aerosol Robotic Network, *Holben et al.*, 1998) observations from Bordj Badji Mokhtar (BBM) on June

17th, 2011. The "desert-dust" RGB composite image (*Lensky and Rosenfeld*, 2008) from SEVIRI at 10:30 UTC is shown alongside. The RGB nicely indicates the position of the dust plume which is also clearly seen in the IASI AOD (Figure 6). It is evident that the IASI retrieval fails to fully reproduce the visible AOD across this thick dust plume (AERONET shows that AOD can exceed 3), but at least the Mie version of the IASI retrieval now approaches the AOD values retrieved from SEVIRI (in contrast to the previous version analysed in *Banks et al.*, 2013). Comparing Figure 9 with the Mie results in Figure 5 it is evident that in the Mie retrieval a secondary dust plume with $AOD_{0.55\mu m}$ of about 1.2 can be identified, which is much weaker in the FTIR results and in the SEVIRI RGB (which quite often fails to appropriately indicate dust presence, especially in the presence of high atmospheric moisture, see e.g. *Brindley et al.*, 2012; *Banks et al.*, 2013).

Comparing IASI and SEVIRI AOD to AERONET Total AOD for eight stations over June 2011 and June 2012 (thus extending the analysis in *Banks et al.*, 2013 to the full Fennec period) yields Figure 10, where the co-located sample sizes are more than doubled compared to *Banks et al.* (2013). The different colours in the scatterplots indicate different atmospheric conditions (see figure caption). Water vapour columns from the European Centre for Medium-range Weather Forecast (ECMWF) ERA-Interim are used for classification of the observations together with SEVIRI 0.6µm albedo (consistent with *Banks et al.*, 2013). All three retrievals have highest RMS under moist conditions (blue and purple symbols), while the overall performance seems to be comparable for all three (the IASI FTIR version has highest overall bias). The underestimation of AOD (negative bias) by the IASI retrievals also is strongest for moist conditions. In contrast to both IASI versions the SEVIRI retrieval tends to generally overestimate AOD (positive bias) in all subsets in this analysis.

In order to further evaluate the IASI datasets and to conclude which spectral set is better suited for characterising airborne dust, the AERONET evaluation has been extended to 73 stations within the dust-belt of the Northern hemisphere (0°-45°N, 80°W-160°E). It includes the year 2009 as well as both months of the Fennec campaign (June 2011, June 2012).

The Mediterranean Sea is covered reasonably well by AERONET observations (Figure 10), while over the Atlantic Ocean and inland Central Asia the coverage is sparse. Nevertheless the distribution of stations should result in different types of dust being sampled (e.g. from the central Sahara to east Asia as well as from close to sources to the far-transport regime samples in the Caribbean), and consequently the comparison should provide a good 'quasi-global' overview of the performance of the retrievals.

The results of the comparison with several AERONET subsets are presented for the Mie and FTIR versions of the IASI retrieval in Table 4. The abbreviations in the table relate to three cases: one using the full IASI retrieval version compared to AERONET AOD (total); one where the full IASI retrieval is evaluated against coarse mode AERONET AOD (CM); and one where the coarse mode AERONET AOD is again used for evaluation, but this time against IASI retrievals where the transfer from the IR to visible optical depth is kept fixed at the average value of 2.69 (average over all size distributions and mixtures) and does not depend on particle size or composition (referred to as “Static Transfer”, ST).

The comparison of IASI Dust AOD with AERONET Total AOD for all stations yields bias and RMSD (Root-Mean-Square Deviation) results comparable to those of the Fennec evaluation alone (Figure 10). The RMSD in the semi-global analysis is slightly smaller for both IASI versions compared to the Fennec analysis, since close to dust source regions for thick dust plumes AOD is underestimated by the IASI retrieval (Figure 9). The evaluation in Table 4 includes a higher fraction of dust observations in the far-range transport field, where AOD is much lower and consequently the RMSD also reduces. It is evident for all three evaluation datasets that the correlation between IASI and AERONET is higher for the FTIR version of the IASI retrieval than for the version using Mie spectra. In terms of bias and RMSD the picture is less clear, but RMSD in particular does not vary much between the FTIR and Mie versions. In terms of correlation, RMSD, bias and fraction of AOD within ±0.2, the comparison with total AERONET AOD yields much worse results than both comparisons with coarse mode AOD. Using a dust property based transfer function for AOD between IR and VIS increases the correlation compared with the use of a static transfer for the FTIR case, while RMSD and AOD±0.2 fraction do not vary strongly.

6 Discussion

Hyperspectral IR retrievals of dust properties strongly depend on the spectral database of optical properties which is used. The optical properties, and consequently retrieval results are also sensitive to the particle size distribution and dust composition. It is therefore not a straightforward task to decide which set of spectral dust properties is the best to use. Figures 1 and 2 indicate that the mineralogical composition of the dust is as important as particle size in determining the shape of the extinction spectra. Because of this, here we have developed two optical property databases to use in conjunction with IASI observations, using mixtures of single components as defined in the literature for different geographical regions and observed atmospheric size distributions. One database is derived from Mie theory and one derived from spectral dust extinction of dust components measured in the laboratory (FTIR).

The comparison of IASI dust AOD retrieved using Mie and FTIR spectra with AERONET and SEVIRI (dust) AOD for June 2011 and 2012 over the western Sahara desert indicates that both versions are capable of identifying the dust plumes and high dust loads observed by the other methods. In contrast to SEVIRI both IASI retrieval versions tend to underestimate dust AOD compared to AERONET Total AOD, especially in moist air. The Fennec (June 2011, 2012) evaluation results suggest that the dependence of retrieval results on surface emissivity (closely linked to albedo in desert areas, see *Banks et al.*, 2013) is more pronounced in the Mie version of the IASI retrieval than in the FTIR version.

The reliability of the assumption that other dust properties in addition to AOD can be retrieved with hyperspectral IR observations can be assessed by comparing the correlation between AERONET and IASI AOD. As seen above, the ratio between AOD_{VIS} and AOD_{IR} is a function of particle size and dust composition, which has been calculated using Mie simulations for both retrieval versions. Using a fixed $\mathrm{AOD_{VIS}/AOD_{IR}}$ ratio (ST in Table 4), calculated as an average over all dust mixtures and size distributions, yields an impression about how much the results are improved by accounting for composition and particle size. The results are listed in Table 4. It is evident that, for the FTIR version, correlation increases when size- and composition-dependent transfer ratios are used. Consequently it can be concluded that the retrieval of particle size and dust mixture adds additional information to the dust retrieval, a result which is strongly supported by *Pierangelo et al.* (2004) and *Clarisse et al.* (2010). On the other hand Figure 7 suggests that, given the different particle sizes and hence IR-VIS transfer coefficients, AOD_{IR} strongly deviates between the Mie and FTIR versions. Consequently it cannot be concluded which infrared AOD is more reliable.

Dust layer height is retrieved only indirectly. From the IASI observations and the optical properties of the dust together with AOD_{IR}, the effective emission temperature of the dust is estimated. Using numerical weather prediction results, here from the WRF model, this temperature can be converted to a dust layer altitude by interpolating between dust temperature and the vertical temperature profile provided by the model simulation. Validation of dust layer altitude has not yet been performed and will be the topic of a subsequent study, where LIDAR observations from satellite and aircraft campaigns will be used to assess the reliability of the retrieved dust layer altitude. Nevertheless, it has been shown by the information content analysis that the signal of dust layer altitude is contained in the observations. In the FTIR version of the IASI retrieval the dust layer altitude looks very plausible (see e.g. overview of dust layer heights in *Tsamalis et al.*, 2013), and values and spatial patterns are within the expected ranges. For the Mie version this conclusion is not true. Dust altitudes seem to be low-biased where most dust in the Mie retrieval does not extend to altitudes of more than 500m above ground. Although the Mie version performs better in the Fennec case in terms of AOD, physical consistency seems to be better in the FTIR version if dust layer altitude is also taken into account.

Comparisons over the Fennec period (June 2011 and 2012) are made with both AERONET observations at BBM and retrievals from SEVIRI. The SEVIRI retrieval method uses infrared brightness temperature differences which are then related to a visible optical depth using fixed bulk aerosol properties (*Brindley and Russell*, 2009). Changes in dust mineralogical composition and particle size thus are not reflected in the SEVIRI results. As SEVIRI lacks the fine spectral resolution analysed here, narrow-band sensors such as SEVIRI may be less sensitive to the choice of dust optical properties than hyperspectral sensors such as IASI.

The comparison of both IASI algorithm versions with AERONET AOD suggests that AERONET coarse mode AOD is better suited for dust AOD evaluation than total AOD, as the statistics show a marked improvement. With respect to the different approaches from IASI, the correlation with AERONET coarse mode AOD improves for the IASI retrieval run with FTIR spectra when the IR-VIS transfer function is calculated from the retrieved dust properties. This implies that particle size and dust composition have a non-negligible influence on the optical properties, especially in the FTIR version. In all three subsets the FTIR version performs better than the Mie version in terms of correlation. Thus it can be concluded that from the two versions used here the FTIR version provides more reliable information about airborne dust. This conclusion is supported by the more plausible distribution of retrieved dust layer heights for the FTIR version. About 85% of IASI observations are within ±0.2 of AERONET coarse mode AOD, but, as evidenced by the Fennec comparison, the IASI retrieval fails to correctly quantify thick dust plumes. This may partly be due to the imperfect knowledge about, and thus the description of, radiance from the surface (the baseline temperature essentially is not equal to the surface temperature as the signal gets saturated at high AOD) as well as to saturation effects. Moreover, the FTIR spectra in particular may fail to correctly describe the extinction by giant dust particles within thick dust plumes given the size distributions of the FTIR samples.

Although the FTIR version in this analysis partly outperforms the Mie version, one should not draw the conclusion that Mie theory is not at all suitable to provide information about desert dust extinction in the thermal infrared. Much of the uncertainty in the Mie spectra is a direct consequence of the imperfect knowledge about refractive indices of minerals (see Figure 1). Consequently, with more reliable refractive indices of major dust components (and higher spectral sampling), optical properties derived from Mie theory should become more reliable.

Unless the reliability of refractive indices is improved, the extinction spectra measured in the laboratory are assumed to be better suited to describing the spectral shape of infrared dust extinction. On the other hand it is also clear that the FTIR samples used here do not cover the full width of particle sizes of airborne dust. Consequently particle sizes in the FTIR version may be low-biased, which has direct consequences for the retrieval of all other dust properties. For sensors with lower spectral resolution (such as SEVIRI), the dependence on the actual spectral shape of extinction is much less and hence describing the infrared optical properties of airborne desert dust with Mie theory may have less impact on retrieval results.

The information spectra of dust extinction clearly show that the information contained in the IASI observations is highest between 1100cm^{-1} and 1200cm^{-1}, where significant variations in spectral surface emissivity, particularly over desert, are also observed (see e.g. *Banks et al.*, 2013). The IASI method used in this study has been developed to minimise the impact of surface emissivity on retrieval results (*Klüser et al.*, 2011; *Klüser et al.*, 2012). Consequently, directly utilising the spectral variation in observed dust-affected radiances instead of creating radiance lookup tables enables the high information content in the spectra to be exploited, despite the imperfect knowledge about the surface emissivity spectrum.

7 Conclusions and outlook

Properties of airborne mineral dust are highly variable in space and time. The extinction signal in hyperspectral infrared observations is affected by changes in dust particle size and dust composition as well as dust loading and height. The information content of infrared dust spectra generated with Mie representations of dust extinction as well as from FTIR laboratory measurements has been analysed with respect to sensitivities to dust properties in this spectral domain. The information content and the number of degrees of freedom for signal differ between spectra simulated with Mie theory and dust extinction spectra measured in the laboratory.

A retrieval algorithm for IASI has been improved to apply both the Mie and FTIR dust spectra in order to quantitatively assess the uncertainty brought about by the use of one set of spectra or the other. Comparison with AERONET and SEVIRI AOD during the Fennec campaign of June 2011 and June 2012 in north-western Africa showed that both versions underestimate dust load, especially for thick dust plumes. Moreover it could be seen that the derived dust properties differ significantly between both versions. The most striking feature is that the dust layer altitude approaches zero over wide parts of the domain for the Mie representation of the dust extinction, indicating that the reliability of the retrieved results might be questionable in this case.

From evaluation with AERONET observations over the global dust-belt domain it can be concluded that using FTIR spectra yields higher correlations with AERONET AOD than using Mie spectra – at similar bias and RMSD. Nevertheless from these results one cannot draw the conclusion that Mie theory is generally insufficient to describe extinction by airborne dust. While in the Rayleigh limit of almost pure absorption by dust other methods are better suited to describe dust extinction (e.g. *Hudson et al.*, 2008a;b), the naturally occurring dust particle size distributions also extend well into the range of Mie scattering. The scattering of IR radiation by dust has to be taken into account in order to correctly describe the spectral variation of dust extinction (e.g. *Dufresne et al.*, 2002), as can be seen by the spectral shape of the dust extinction spectra for different size distributions. However, we have also shown that the selection of refractive indices from one source or another itself introduces sizeable uncertainties which may overwhelm the drawbacks of approximating dust particles as spheres. Consequently Mie theory may still be appropriate for describing the impact of airborne dust on the radiance field, if reliable optical properties for dust components (in the relevant particle size range) become available. Further research on the description of optical properties of dust components for realistic dust particle size distributions is obviously needed.

The selection of AERONET data also affects evaluation results. We show that the coarse mode AOD is much better suited to describe AOD of airborne dust than the total AOD. Using a size- and composition-dependent transfer function from IR to VIS in the IASI retrieval also adds valuable information and can increase correlation with AERONET coarse mode AOD. Although this result cannot be regarded as an evaluation of particle size and composition of the dust, it shows that the information is contained in the IASI spectra and moreover that it is being used appropriately.

The impact of surface emissivity is strongest at wavenumbers between 1075cm^{-1} and 1250cm^{-1} (see *Klüser et al.*, 2011; *Banks et al.*, 2013), where the information content with respect to dust is highest. Observations from 830-990cm^{-1} can add extra information but these are more strongly affected by water vapour. Consequently, the full spectral range of the atmospheric window should be exploited for inferring dust information, as neither of the two window bands separated by the ozone absorption band carries a pure dust signal. In a future study it will be assessed how spectral information on surface emissivity (ideally from the binned IASI spectra themselves) can be used to reduce the emissivity signal and consequently to further increase the quality of the optical depth retrieval.

Campaign data and LIDAR measurements will also be used in further studies for the evaluation of dust properties such as particle size, mineralogical composition and dust layer altitude. From both theoretical considerations and the initial results presented here, information on these parameters is available. Future work will be dedicated to quantifying the reliability of the extraction of this additional information.

The IASI dust observations used in this study (the year 2009 as well as for the Fennec campaign months) are available online in the World Data Center for Remote Sensing of the Atmosphere (WDC-RSAT) mandated by ICSU and the WMO and hosted at the German Remote Sensing Datacenter (DLR-DFD). They can be accessed at http://wdc.dlr.de.

Acknowledgements

We are especially thankful to Paul D. Kleiber and Vicki H. Grassian from the University of Iowa for providing the FTIR spectra and related information as well as for their very fruitful comments on an early version of this paper. We thank all AERONET station Principal Investigators and their staff for establishing and maintaining the 73 AERONET sites used for evaluation and for providing the observation data. We are thankful to EUMETSAT and the EUMETSAT Data Centre (UMARF) for providing the IASI observations form METOP. We thank the anonymous reviewer for very constructive comments which helped substantially in improving the manuscript.

References

Ackerman, S.A.: Remote sensing aerosols using satellite infrared observations, J. Geophys. Res., 102, 17069-17079, 1997.

Adedokun, J.A., Emofurieta, W.O., and Adedeji, O.A.: Physical, Mineralogical and Chemical Properties of Harmattan Dust at Ile-Ife, Nigeria, Theor. Appl. Climatol., 40, 161-169, 1989.

Alexander, J.M., Laksina, O., Meland, B., Young, M.A., Grassian, V.H., and Kleiber, P.D.: A combined laboratory and modeling study of the infrared extinction and visible light scattering properties of mineral dust aerosol, J. Geophys. Res. Atm., 118, 1-18, doi:10.1029/2012JD018751, 2013.

Aronson, J.R., and Strong, P.F.: Optical constants of minerals and rocks, Appl. Opt., 14, 2914-2920, 1975.

Aronson, J.R., Emslie, A.G., Smith, E.M., and Strong, P.F.: Infrared spectra of lunar soils and related optical constants, Proc. Lunar Planet. Sci. Conf. 10th, 1787-1795, 1979.

Aronson, J.R.: Optical constants of monoclinic anisotropic crystals: orthoclase, Spectrochimica Acta, 42A, 187-190, 1986.

Balkanski, Y., Schulz, M., Claquin, T., and Guibert, S.: Reevaluation of Mineral aerosol radiative forcings suggests a better agreement with satellite and AERONET data, Atmos. Chem. Phys., 7, 81-95, 2007.

Banks, J. R. and Brindley, H. E.: Evaluation of MSG-SEVIRI mineral dust retrieval products over North Africa and the Middle East, Remote Sens. Environ., 128, 58-73, doi:10.1016/j.rse.2012.07.017, 2013.

Banks, J.R., Brindley, H.E., Flamant, C., Garay, M.J., Hsu, N.C., Kalashnikova, O.V., Klüser, L., and Sayer, A.M.: Intercomparison of satellite dust retrieval products over the west African Sahara during the Fennec campaign in June 2011, Remote Sens. Environ., 136, 99-116, 2013.

Brindley, H.E., and Russell, J.E.: Improving GERB scene identification using SEVIRI: Infrared dust detection strategy, Remote Sens. Environ., 104, 426-446, 2006.

Brindley, H.E., and Russell, J.E.: An assessment of Saharan dust loading and the corresponding cloud-free longwave direct radiative effect from geostationary satellite observations, J. Geophys. Res., 114, D23201, doi:10.1029/2008JD011635, 2009.

Brindley, H.E., Knippertz, P., Ryder, C., and Ashpole, I.: A critical evaluation of the ability of the Spinning Enhanced Visible and Infrared Imager (SEVIRI) thermal infrared red-green-blue rendering to identify dust events: Theoretical analysis, J. Geophys. Res., 117, D07201, doi:10.1029/2011JD017326, 2012.

Caquineau, S., Gaudichet, A., Gomes, L., Magonthier, M.-C., and Chatenet, B.: Saharan dust: Clay ratio as a relevant tracer to assess the origin of soil-derived aerosols, Geophys. Res. Lett., 25, 983-986, 1998.

Clarisse, L., Hurtmans, D., Prata, A.J., Karagulian, F., Clerbaux, C., De Mazière, M., and Coheur, P.-F.: Retrieving radius, concentration, optical depth, and mass of different types of aerosols from high-resolution infrared nadir spectra, Appl. Opt., 49, 3713-3722, 2010.

Clarisse, L., Coheur, P.-F., Prata, F., Hadji-Lazaro, J., Hurtmans, D., and Clerbaux, C.: A unified approach to infrared aerosol remote sensing and type specification, Atmos. Chem. Phys., 13, 2195-2221, 2013.

De Leeuw, G., et al.: Evaluation of seven European aerosol optical depth retrieval algorithms for climate analysis, Remote Sens. Environ., doi:10.1016/j.rse.2013.04.023, 2013.

DeSouza-Machado, S.G., Strow, L.L., Imbiriba, B., McCann, K., Hoff, R.M., Hannon, S.E., Martins, J.V., Tanré, D., Deuzé, J.L., Ducos, F., and Torres, O.: Infrared retrievals of dust using AIRS: Comparisons of optical depths and heights derived for a North African dust storm to other collocated EOS A-Train and surface observations, J. Geophys. Res., 115, D15201, doi:10.1029/2009JD012842, 2010.

Dubovik, O., Holben, B.N., Eck, T.F., Smirnov, A., Kaufman, Y.J., King, M.D., Tanré, D., and Slutsker, I.: Variability of Absorption and Optical Properties of Key Aweosol Types Observed in Worldwide Locations, J. Atmos. Sci., 59, 590-608, 2002.

Dubovik, O., Sinyuk, A., Lapyonok, T., Holben, B.N., Mishchenklo, M., Yang, P., Eck, T.F., Volten, H., Munoz, O., Veihelmann, B., van der Zande, W.J., Leon, J.-F., Sorokin, M., ald Slutsker, I.: Application of spheroid models to account for aerosol particle nonsphericity in remote sensing of desert dust, J. Geophys. Res., 111, D11208, doi:10.1029/2005JD006619, 2006.

Dufresne, J.-L., Gautier, C., Ricchiazzi, P., and Fouquart, Y.: Longwave scattering effects of mineral aerosols, J. Atmos. Sci., 59, 1959-1966, 2002.

Engelbrecht, J.P., McDonald, E.V. Gillies, J.A., Jayanty, R.K.M., Casuccio, G., and Gertler, A.W.: Characterizing Mineral Dusts and Other Aerosols from the Middle East – Part 1: Ambient Sampling, Inh. Toxicol., 21, 297-326, 2009.

Foner, H.A., and Ganor, E.: The chemical and mineralogical composition of some urban atmospheric aerosols in Israel, Atm. Env., 26B, 125-133, 1992.

Glaccum, R.A., and Prospero, J.M.: Saharan aerosols over the tropical North Atlantic – Mineralogy, Marine Geology, 37, 295-321, 1980.

Glotch, T.D., Rossman, G.R., and Aharonson, O.: Mid-infrared (5-100μm) reflectance spectra and optical constants of ten phy´llosilicate minerals, Icarus, 192, 605-622, 2007.

Haywood 2003, J.M., Francis, P.N., Osborne, S.R., Glew, M.D., Loeb, N., Highwood, E.J., Tanré, D., Myhre, G., Formenti, P., and Hirst, E.: Radiative properties and direct radiative effect of Saharan dust measured by the C-130 aircraft during SHADE: 1. Solar spectrum, J. Geophys. Res., 108, doi:10.1029/2002JD002687, 2003.

Haywood, J.M., Johnson, B.T., Osborne, S.R., Baran, A.J., Brooks, M., Milton, S.F., Mulcahy, J., Walters, D., Allan, R.P., Klaver, A., Formenti, P., Brindley, H.E., Christopher, S., and Gupta, P.: Motivation, rationale and key results from the GERBILS Saharan dust measurement campaign, Q. J. Royal Meteorol. Soc., 137, 1106-1116, 2011.

Hess, M. Koepke, P.,and Schult, I.: Optical Properties of Aerosols and Clouds: The Software Package OPAC, Bull. Am. Meteorolog. Soc., 79, 831-844, 1998.

Highwood, E., Haywood, J., Silverstone, M., Newman, S., and Taylor, J.: Radiative properties and direct effect of Saharan dust measured by the C-130 aircraft during Saharan Dust Experiment (SHADE): 2. Terrestrial spectrum, J. Geophys. Res., 108(D18), 8578, doi:10.1029/2002JD002552, 2003.

Holben, B.N., Eck, T.F., Slutsker, I., Tanré, D., Buis, J.P., Setzer, K.A., Vermote, E., Reagan, J.A., Kaufman, Y.J., Nakajima, T., Lavenu, F., Jankowiak, I., and Smirnov, A.: AERONET - A Federated Instrument Network and Data Archive for Aerosol Characterization, Remote Sens. Environ., 66, 1-16, 1998.

Hudson, P. K., Young, M. A., Kleiber, P. D., and Grassian, V. H.: Coupled infrared extinction spectra and size distribution measurements for several non-clay components of mineral dust aerosol (quartz, calcite, and dolomite), Atm. Environ., 42, 5991-5999, 2008a.

Hudson, P. K., Gibson, E. R., Young, M. A., Kleiber, P. D., and Grassian, V. H.: Coupled infrared extinction and size distribution measurements for several clay components of mineral dust aerosol, J. Geophys. Res., 113, D01201, doi:10.1029/2007JD008791, 2008b.

Hulley, G.C., Hook, S.J., Manning, E., Lee, S.-Y., and Fetzer, E.: Validation of the Atmospheric Infrared Sounder (AIS) version 5 land surface emissivity product over the Namib and Kalahari deserts, J. Geophys. Res., 114, D19104, doi:10.1029/2009JD012351, 2009.

Jeong, G.Y.: Bulk and single-particle mineralogy of Asian dust and a comparison with its source soils, J. Geophys. Res., 113, D02208, doi:10.1029/2007JD008606, 2008.

Jeong, G.Y., Choi, J.-H., Lim, H.S., Seong, C., and Yi, S.B.: Deposition and weathering of Asian dust in Paleolithic sites, Korea, Quarternary Science Reviews, 78, 283-300, 2013.

Johnson, B.T., and Osborne, S.R.: Physical and optical properties of mineral dust aerosol measured by aircraft during the GERBILS campaign, Q. J. R. Meteorolog. Soc., doi:10.1002/qj.777, 2011.

Kahlaf, F.I., Al-Kadi, A., and Al-Saleh, S.: Mineralogical composition and potential sources of dust fallout deposits in Kuwait, Northern Arabian Gulf, Sedimentary Geology, 42, 255-278, 1985.

Kandler, K., Benker, N., Bundke, U., Cuevas, E., Ebert, M., Knippertz, P., Rodriguez, S., Schütz, L., and Weinbruch, S.: Chemical composition and complex refractive index of Saharan Mineral Dust at Izana, Tenerife (Spain) derived by electron microscopy, Atm. Env., 41, 8058-8074, 2007.

Kandler, K., Schütz, L., Deutscher, C., Ebert, M., Hofmann, H., Jäckel, S., Jaenicke, R., Knippertz, P., Lieke, K., MAssling, A., Petzold, A., Schladitz, A., Weinzierl, B., Wiedensohler, A., Zorn, S., and Weinbruch, S.: Size distribution, mass concentration, chemical and mineralogical composition and derived optical parameters of the boundary layer aerosol at Tinfou, Morocco, during SAMUM 2006, Tellus, 61B, 32-50, 2009.

Kandler, K., Schütz, L., Jäckel, S., Lieke, K., Emmel, C., Müller-Ebert, D., Ebert, M., Scheuvens, D., Schladitz, A., Šegvić, B., Wiedensohler, A., and Weinbruch, S.: Ground-based off-line aerosol measurements at Praia, Cape Verde during the Saharan Mineral Dust Experiment: microphysical properties and mineralogy, Tellus, 63B, 459-474, 2011.

Kleinman, D.A., and Spitzer, W.G.: Theory of the Optical Properties of Quartz in the Infrared, Phys. Rev., 125, 16-30, 1962.

Klüser, L., and Schepanski, K.: Remote sensing of mineral dust over land with MSG infrared channels: A new Bitemporal Mineral Dust Index, Remote Sens. Environ., 113, 1853-1867, 2009.

Klüser, L., Martynenko, D., and Holzer-Popp, T.: Thermal infrared remote sensing of mineral dust over land and ocean: a spectral SVD based retrieval approach for IASI, Atmos. Meas. Tech., 4, 757-773, doi:10.5194/amt-4-757-2011, 2011.

Klüser, L., Kleiber, P., Holzer-Popp, T., and Grassian, V.H.: Desert dust observation from space – Application of measured mineral component infrared extinction spectra, Atm. Env., 54, 419-427, 2012.

Koike, C., Hasegawa, H., Asada, N., and Komatuzaki, T.: Optical constants of fine particles for the infrared region, Mon. Not. R. astr. Soc., 239, 127-137, 1989.

Koike, C., and Shibai, H.: Optical constants of hydrous silicates from 7 to 400 µm, Mon. Not. R. astr. Soc., 246, 332-336, 1990.

Koren, I., Kaufman, Y.J., Washington, R., Todd, M.C., Rudich, Y., Vanderlei Martins, J., and Rosenfeld, D.: The Bodélé depression: a single spot in the Sahara that provides most of the mineral dust to the Amazon forest, Environ. Res. Lett., 014005, doi:10.1088/1748-9326/1/1/014005, 2006.

Laksina, O., Young, M.A., Kleiber, P.D., and Grassian, V.H.: Infrared extinction spectra of mineral dust aerosol: Single components and complex mixtures, J. Geophys. Res., 117, D18210, doi: 10.1029/2012JD017756, 2012.

Legrand, M., Plana-Fattori, A., and N'doume, C.: Satellite detection of dust using the IR imagery of Meteosat, 1. Infrared Difference Dust Index. J. Geophys. Res., 106(D16), 18251−18274, 2001.

Lensky, I. M., and Rosenfeld, D.: Clouds–Aerosols–Precipitation Satellite Analysis Tool (CAPSAT), Atm. Chem. Phys., 8, 6739–6753, 2008.

Longtin, D.R., Shettle, E.P., Hummel, J.R., and Pryce, J.D.:,A wind dependent desert aerosol model: Radiative properties, AFGL-TR-88-0112, Air Force Geophysics Laboratory, Hanscom Air Force Base, Lincoln, Mass., 1988.

Mahowald, N. M., Baker, A. R., Bergametti, G., Brooks, N., Duce, R. A., Jickells, T. D., et al. : Atmospheric global dust cycle and iron inputs to the ocean. Global Biogeochemical Cycles, 19, GB4025. doi:10.1029/2004GB002402, 2005.

Martynenko, D., Holzer-Popp, T., Elbern, H., and Schroedter-Homscheidt, M.: Understanding the aerosol information content in multi-spectral reflecance measurements using a synergetic retrieval algorithm, Atmos. Meas. Tech., 3, 1589-1598, 2011.

Marzo, G.A., Blanco, A., De Carlo, F., D'Elia, M., Fonti, S., Marra, A.C., Orofino, V., and Politi, R.: The optical constants of gypsum particles as analog of Martian sulfates, 2004.

McConnell, C.L., Highwood, E.J., Coe, H., Formenti, P., Anderson, B., Osborne, S., Nava, S., Desboeufs, K., Chen, G., and Harrison, M.A.J.: Seasonal variations of the physical and optical characteristics of Saharan dust: Results from the Dust Outflow and Deposition to the Ocean (DODO) experiment, J. Geophys. Res., 113, D14S05, doi:10.1029/2007JD009606, 2008.

Menke, W.: Geophysical Data Analysis: Discrete Inverse Theory, 3rd Edition, Academic Press, Waltham, MA, USA, 2012.

Mogili, P.K., Yang, K.H., Young, M.A., Kleiber, P.D., and Grassian, V.H.: Extinction spectra of mineral dust aerosol components in an environmental aerosol chamber: IR resonance studies, Atm. Env., 42, 1752-1761, 2008.

Mutschke, H., Begemann, B., Dorschner, J., Gürtler, J., Gustafson, B., Henning, T., and Stognienko, R.: Steps toward interstellar silicate mineralogy III. The role of aluminium in circumstellar amorphous silicates, Astron. Astrophys., 333, 188-198, 1998.

O'Neill, N.T., Eck, T.F., Smirnov, A., Holben, B.N., and Thulasiraman, S.: Spectral discrimination of coarse and fine mode optical depth. J. Geophys. Res. 108 (D17), 4559-4573, doi:10.1029/2002JD002975, 2003.

Orofino, V., Blanco, A., Fonti, S., Marra, A.C., and Polimeno, N.: The complex refractive index of limestone particles: an extension to the FIR range for Mars applications, Planetary and Space Science, 50, 839-847, 2002.

Osborne, S.R., Johnson, B.T., Jaywood, J.M., Baran, A.J., Harrison, M.A.J., and McConnell, C.L.: Physical and optical properties of mineral dust aerosol during the Dust and Biomass-burning Experiment, J. Geophys. Res., 113, doi:10.1029/2007JD009551, 2008.

Pavolonis, M. J., Heidinger, A.K., and Sieglaff, J.: Automated retrievals of volcanic ash and dust cloud properties from upwelling infrared measurements, J. geophys. Res. Atmos., 118, 1-23, doi:10.1002/jgrd.50173, 2013.

Peterson, J.T., and Weinman, J.A.: Optical properties of quartz dust particles at infrared wavelengths, J. Geophys. Res., 74, 28, 6947-6952, 1969.

Pierangelo, C., Chédin, A., Heiliette, S., Jacquinet-Husson, N., and Armante, R.: Dust altitude and infrared optical depth from AIRS, Atmos. Chem. Phys., 4, 1813-1822, doi:10.5194/acp-4-1813-2004, 2004.

Prospero, J.M.: Long-range transport of mineral dust in the global atmosphere: Impact of African dust on the environment of the southeastern United States, Proc. Natl. Acad. Sci. USA, 96, 3396-3403, 1999.

Quenzel, H. and Müller, H.: Optical Properties of Single Mie Particles: Diagrams of Intensity- Extinction- Scattering- and Absorption Efficiencies, Wiss. Mit. Nr. 34, Universitaet Muenchen, 59pp., 1987.

Rashki, A., Eriksson, P.G., Rautenbach, C.J. de W., Kaskaoutis, D.G., Grote, W., and Dykstra, J.: Assessment of chemical and mineralogical characteristics of airborne dust in the Sistan region, Iran, Chemosphere, doi:10.1016/j.chemosphere.2012.06.059, 2012 (in press).

Rodgers, C.D.: Information content and optimization of high spectral resolution remote measurements, Adv. Space Res., 21, 361-367, 1998.

Rodgers, C. D.: Inverse methods for atmospheric sounding, Theory and practice, in: Series on Atmospheric, Oceanic and Planetary Physics, vol. 2, World Scientific Publishing, Singapore, 2000.

Russell, E.E., and Bell, E.E.: Measurement of the optical constants of crystal quartz in the far infrared with the asymetric Fourier-Transform method, Journal of the Optical Society of America, 57, 3, 341-348, 1967.

Ryder, C.L., Highwood, E.J., Rosenberg, P.D., Trembath, J., Brooke, J.K., Bart, M., Dean, A., Crosier, J., Dorsey, J., Brindley, H., Banks, J., Marsham, J.H., McQuaid, J.B., Sodemann, H., and Washington, R.: Optical properties of Saharan dust aerosol and contribution from the coarse mode as measured during the Fennec 2011 aircraft campaign, Atmos. Chem. Phys., 13, 303-325, 2013.

Salisbury, J.W., and Wald, A.: The role of volume scattering in reducing spectral contrast of Reststrahlen bands in spectra of powdered minerals, Icarus, 96, 121-128, 1992.

Schroedter-Homscheidt, M., Oumbe, A., Benedetti, A., and Morcrette, J.-J.: Aerosols for Concentrating Solar Electricity Production Forecasts: Requirement Quantification and ECMWF/MACC Aerosol Forecast Assessment. Bull. Amer. Meteor. Soc., 94, 903–914, 2013.

Shannon, C.E., and Weaver, W.: The Mathematical Theory of Communication, University of Illinois Press, 1949.

Shao, L.Y., Li, W.J., Yang, S.S., Shi, Z.B., and Lü, S.L.: Mineralogical characteristics of airborne particles collected in Beijing during a severe Asian dust storm period in spring 2002, Sci. China Ser. D-Earth Sci., 50, 953-959, 2007.

Shenk, W.E., and Curran, R.J.: The Detection of Dust Storms Over Land and Water With Satellite Visible and Infrared Measurements, Mon. Weath. Rev., 102, 830-837, 1974.

Skamarock, W. C., Klemp, J. B., Dudhia, J., Gill, D. O., Barker, D. M., Duda, M. G., Huang, X.-Y., Wang, W., and Powers, J. G.: A Description of the Advanced Research WRF Version 3, Technical Note TN-475+STR, NCAR, doi:10.5065/D68S4MVH, 2008.

Slingo, A., Ackerman, T.P., Allan, R.P., Kassianov, E.I., McFarlane, S.A., Robinson, G.J., Barnardm J.C., Miller, M.A., Harries, J.E., Russell, J.E., and Dewitte, S.: Observations of the impact of a major Saharan dust storm on the atmospheric radiation balance, Geophys. Res. Lett., 33, L24817, doi:10.1029/2006GL027869, 2006.

Sokolik, I.N., and Toon, O.B.: Incorporation of mineralogical composition into models of the radiative properties of mineral aerosol from UV to IR wavelengths, J. Geophys.Res., 104, D8, 9423-9444, 1999.

Spitzer, W.G., and Kleinman, D.A.: Infrared lattice bands of quartz, Phys. Rev., 121, 1324-1335, doi:10.1103/PhysRev.121.1324, 1961.

Steyer, T.R., Day, K.L., and Huffman, D.R.: Infrared absorption by small amorphous quartz spheres, Appl. Opt., 13, 7, 1586-1590, 1974.

Tsamalis, C., Chédin, A., Pelon, J., and Capelle, V.: The seasonal vertical distribution of the Saharan Air Layer and its modulation by the wind, Atmos. Chem. Phys., 13, 11235-11257, 2013.

Vandenbussche, S., Kochenova, S., Vandaele, A.C., Kumps, N., and De Mazière, M.: Retrieval of desert dust aerosol vertical profiles from IASI measurements in the TIR atmospheric window, Atmos. Meas. Tech., 6, 2577-2591, 2013.

Washington, R., Todd, M., Middleton, N.J., and Goudie, A.S.: Dust-Storm Source Areas Determined by the Total Ozone Monitoring Spectrometer and Surface Observations, Annals of the Association of American Geographers, 93 (2), 297–313, 2003.

Weinzierl, B., Petzold, A., Esselborn, M., Wirth, M., Rasp, K., Kandler, K., Schütz, L., Koepke, P., and Fiebig, M.: Airborne measurements of dust layer properties, particle size distribution and mixing state of Saharan dust during SAMUM 2006, Tellus, 61B, 96-117, 2009.

Wenrich, M.L., and Christensen, P.R.: Optical constants of minerals derived from emission spectroscopy: Application to quartz, J. Geophys. Res., 101, B7, 15921-15931, 1996.

Yang, P., Wei, H., Huang, H.-L., Baum, B.A., Hu, Y.X., Kattawar, G.W., Mishchenko, M.I., and Fu, Q.: Scattering and absorption property database for nonspherical ice particles in the near- through far-infrared spectral region, Appl. Opt., 44, 5512-5523, 2003.

Yang, P., Feng, Q., Hong, G., Kattawar, G.W., Wiscombe, W.J., Mishchenko, M.I., Dubovik, O., Laszlo, I., and Sokolik, I.N.: Modeling of the scattering and radiative properties of nonspherical dust-like aerosols, Journal of Aerosol Science, 28, 995-1014, 2007.

Tables

Table 1: Names, references, number of modes and mass-weighted mean diameter for the eight dust size distributions used for Mie simulations.

Campaign / Source	**Reference**	**Lognormal Modes**	**D_w**
DODO	*McConnell et al.* (2008)	4	0.93µm
Gen. DABEX	*Osborne et al.* (2008)	2 (generic distribution)	2.18µm
OPAC MITR	*Hess et al.* (1998)	1	2.53µm
GERBILS	*Johnson and Osborne* (2011)	4	2.78µm
Aerosol_CCI	*De Leeuw et al.* (2013)	1	4.69µm
SAMUM-1	*Weinzierl et al.* (2009)	4	6.40µm
SAMUM-2	*Kandler et al.* (2011)	4	11.05µm
Fennec	*Ryder et al.* (2013)	4	12.98µm

Table 2: References for dust composition (left columns) and optical constants (right columns) of desert dust used in this study.

Mixture	Reference		Component	Refractive index reference
China	*Shao* (2007), *Jeong* (2008), Jeong et al. (2013)		***Quartz***	*Peterson and Weinman* (1969)
Iran	*Rashki et al.* (2012)		***Illite*** ***Muscovite***	*Glotch et al.* (2007) *Aronson and Strong* (1975)
Kuwait	*Kahlaf et al.* (1985)		***Kaolinite***	*Glotch et al.* (2007)
Israel	*Foner and Ganor* (1992)		***Montmorillonite***	*Glotch et al.* (2007)
Central Sahara	*Laksina et al.* (2012)		***Chlorite***	*Koike and Shibai* (1990)
Nigeria	*Adedokun et al.* (1989)		***Gypsum***	*Marzo et al.* (2004)
Morocco	*Kandler et al.* (2009)		***Carbonates (Calcite)***	*Orofino et al.* (2002)
Tropical Atlantic	*Claccum and Prospero* (1980)		***Feldspars (bytownite, orthoclase, albite)***	*Aronson et al.* (1979), *Aronson* (1986), *Mutschke et al.* (1998)

Table 3: Typical desert dust compositions as reported in the literature (references in Table 2; N/R: not reported). Presented percentages are calculated by weight. The carbonates include calcite and dolomite, while feldspars include potassium-feldspar (represented by orthoclase in the spectral optical properties) as well as plagioclase.

	Quartz	***Illite / Muscov.***	***Kaol.***	***Montm.***	***Chlorite***	***Gypsum***	***Carb.***	***Feldsp.***
China	25.2%	24.9%	3.1%	20.3%	3.6%	0.4%	9.7%	12.8%
Iran	40.1%	10.2%	N/R	N/R	6.3%	2.0%	24.0%	17.4%
Kuwait	30.6%	4.5%	0.4%	2.4%	0.1%	6.7%	45.1%	10.2%
Israel	23.0%	N/R	N/R	N/R	N/R	2.0%	70.0%	5.0%
C. Sahara	1.4%	31.3%	16.2%	33.6%	N/R	N/R	8.8%	8.7%
Nigeria	70.2%	2.3%	11.0%	N/R	N/R	N/R	N/R	16.5%
Morocco	24.0%	27.0%	4.0%	N/R	3.0%	N/R	14.0%	28.0%
Trop. Atl.	14.2%	62.0%	7.1%	N/R	4.2%	N/R	6.9%	5.6%

Table 4: Correlation coefficient, RMSD, bias, Fraction of IASI AOD within AERONET AOD±0.2 and sample size for comparisons of different algorithm versions with AERONET L1.5 AOD (2009, June 2011/2012). See text for abbreviation of the different sets.

	Mie total	***FTIR total***	***Mie ST***	***FTIR ST***	***Mie CM***	***FTIR CM***
Correlation	0.57	0.61	0.68	0.69	0.67	0.73
RMSD	0.31	0.36	0.17	0.17	0.18	0.18
Bias	-0.17	-0.25	0.00	0.01	0.01	-0.07
$F_{AOD\pm0.2}$	66%	53%	84%	88%	85%	85%
N	824	822	824	822	824	822

Figures

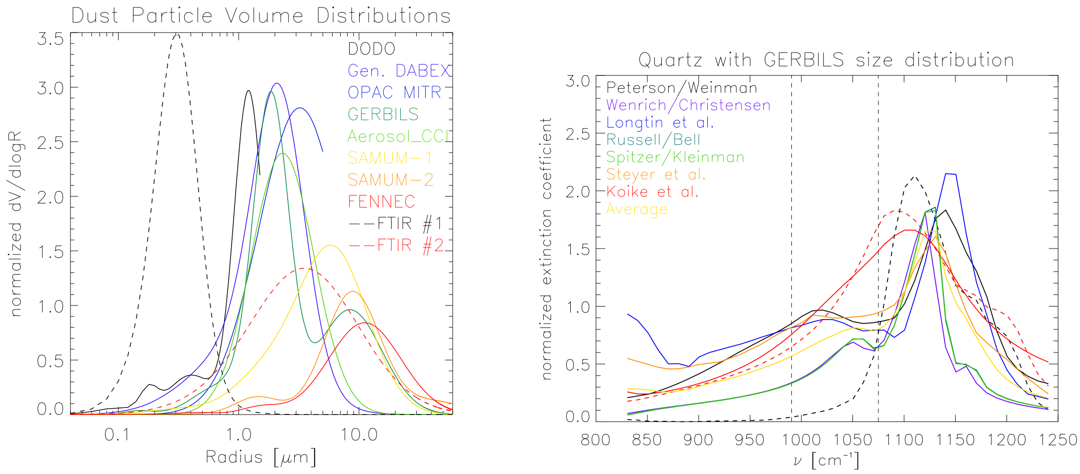

Figure 1: Left: Dust volume size distributions from campaign data (solid) and averaged FTIR samples (dashed). Right: Quartz extinction spectra for the GERBILS size distribution (Tab. 1) calculated with Mie theory and refractive indices from different sources. The black and red dashed curves represent FTIR measurements of the samples #1 and #2, respectively (see text for description of the FTIR samples). The vertical dashed lines bound the ozone absorption band not used for dust retrieval. Running from top to bottom the blue shifts of the different refractive index datasets relative to the FTIR results are 50cm^{-1}, 30cm^{-1}, 50cm^{-1}, 40cm^{-1}, 40cm^{-1}, 40cm^{-1}, 10cm^{-1}, 30cm^{-1} .

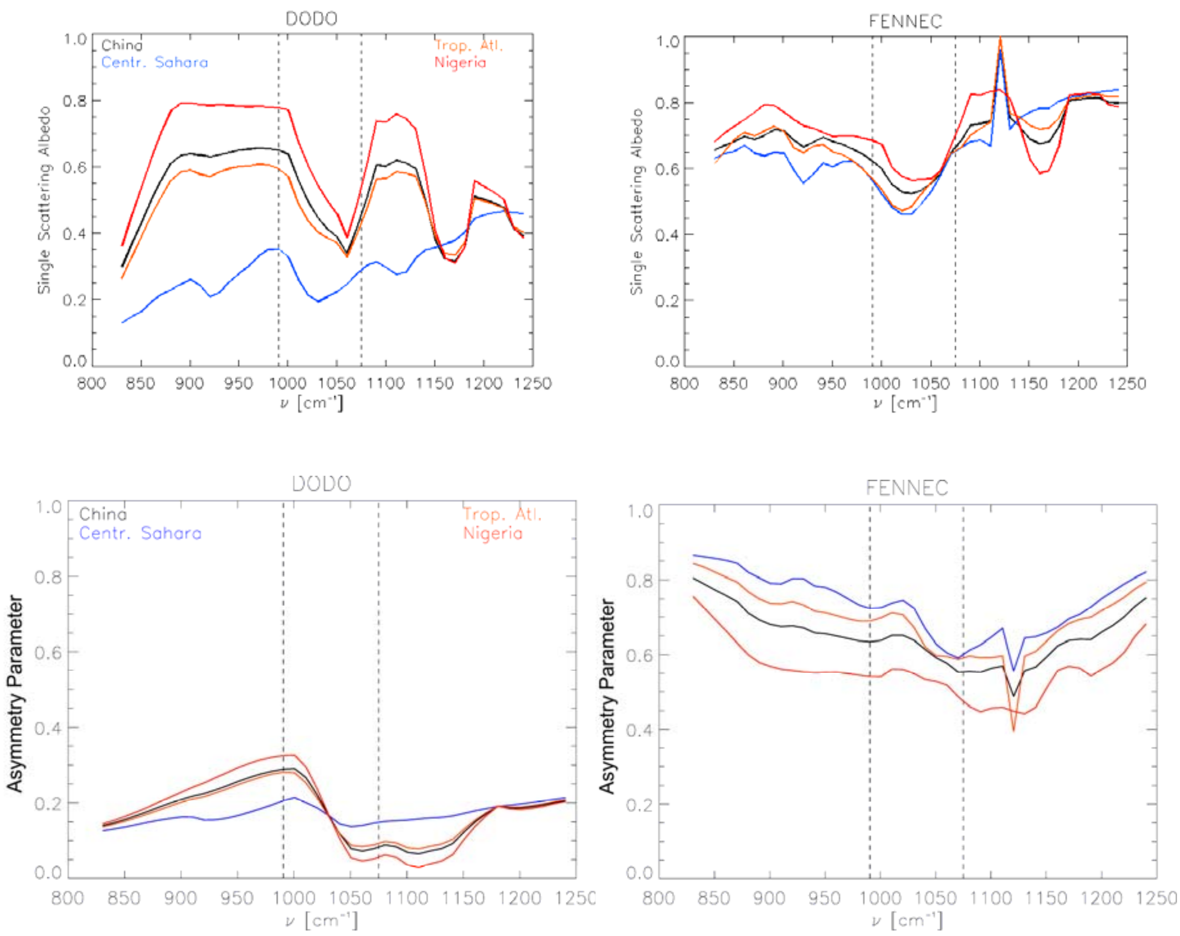

Figure 2: Single scattering albedo (top row) and asymmetry parameter (bottom row) for the China, Central Sahara, Tropical Atlantic and Nigeria dust mixtures using Mie simulations. The left side represents the DODO size distribution and the right side refers to the Fennec size distribution. The vertical dashed lines again represent the boundaries of the ozone absorption band not used for dust retrieval.

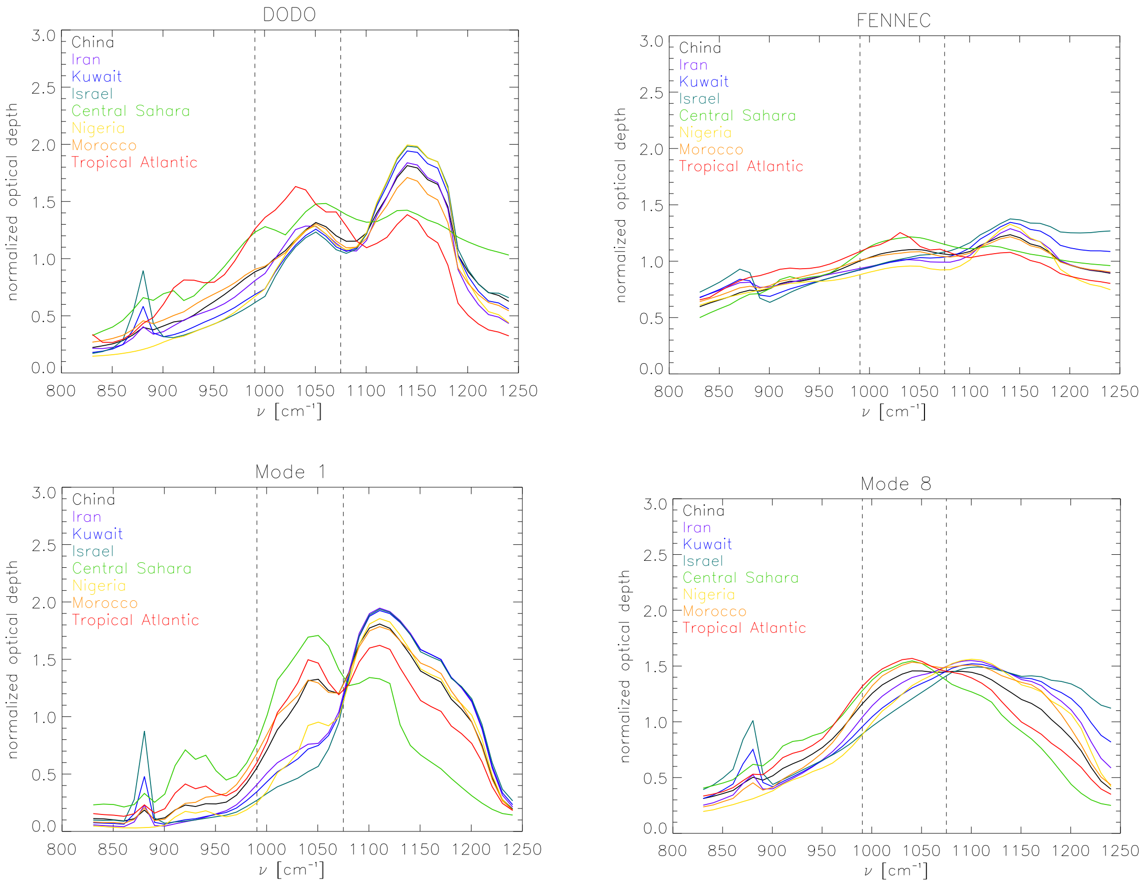

Figure 3: Normalised (to the average of from 925cm^{-1} and 1125cm^{-1})optical depth spectra calculated with the Two-Stream approximation using Mie spectra for the DODO (top left) and Fennec (top right) particle size distributions (Tab. 1) as well as using FTIR spectra for the smallest (bottom left) and largest (bottom right) size mode (sample #1 and #2, respectively).

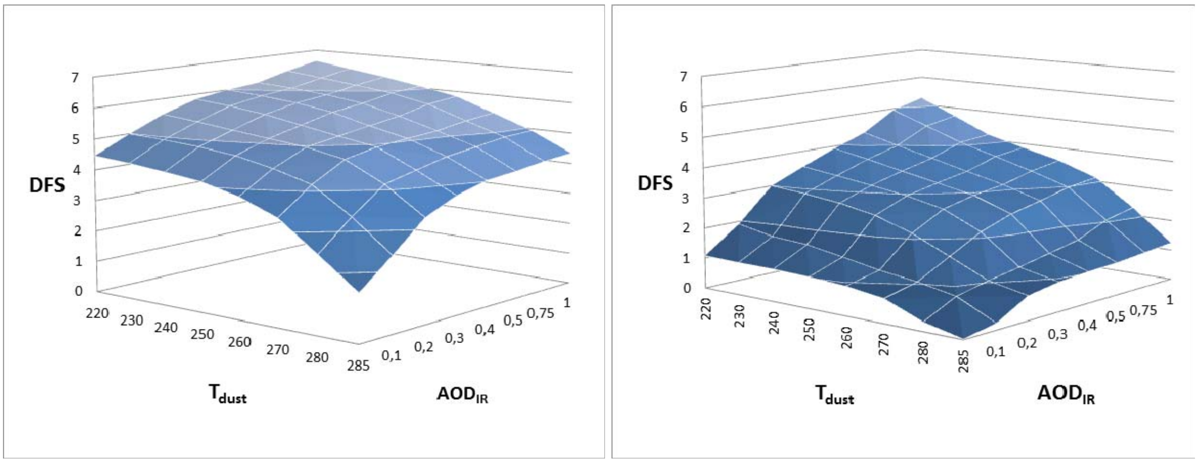

Figure 4: Degrees of freedom for signal calculated for the Mie (left) and FTIR (right) spectra, in relation to AOD_{IR} and dust layer temperature, T_{dust}

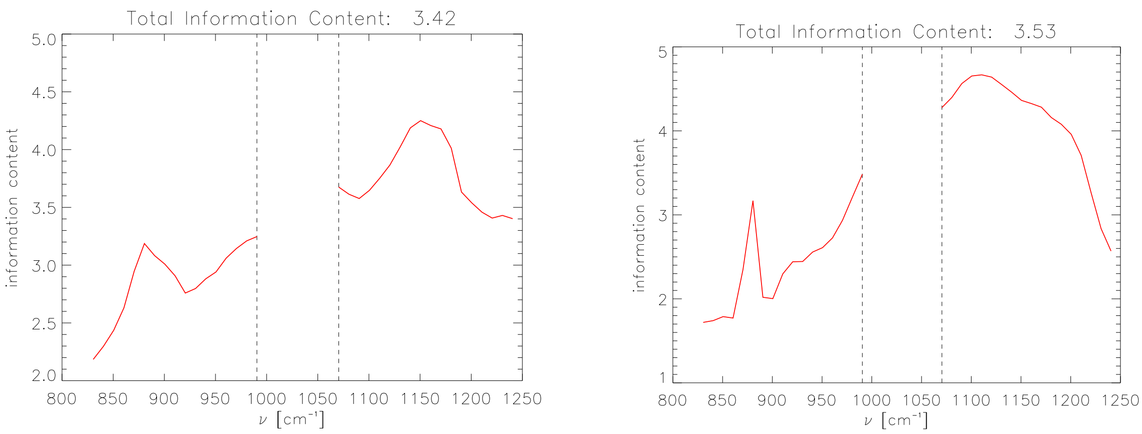

Figure 5: Information spectra of the Mie (left) and FTIR (right) dust representations

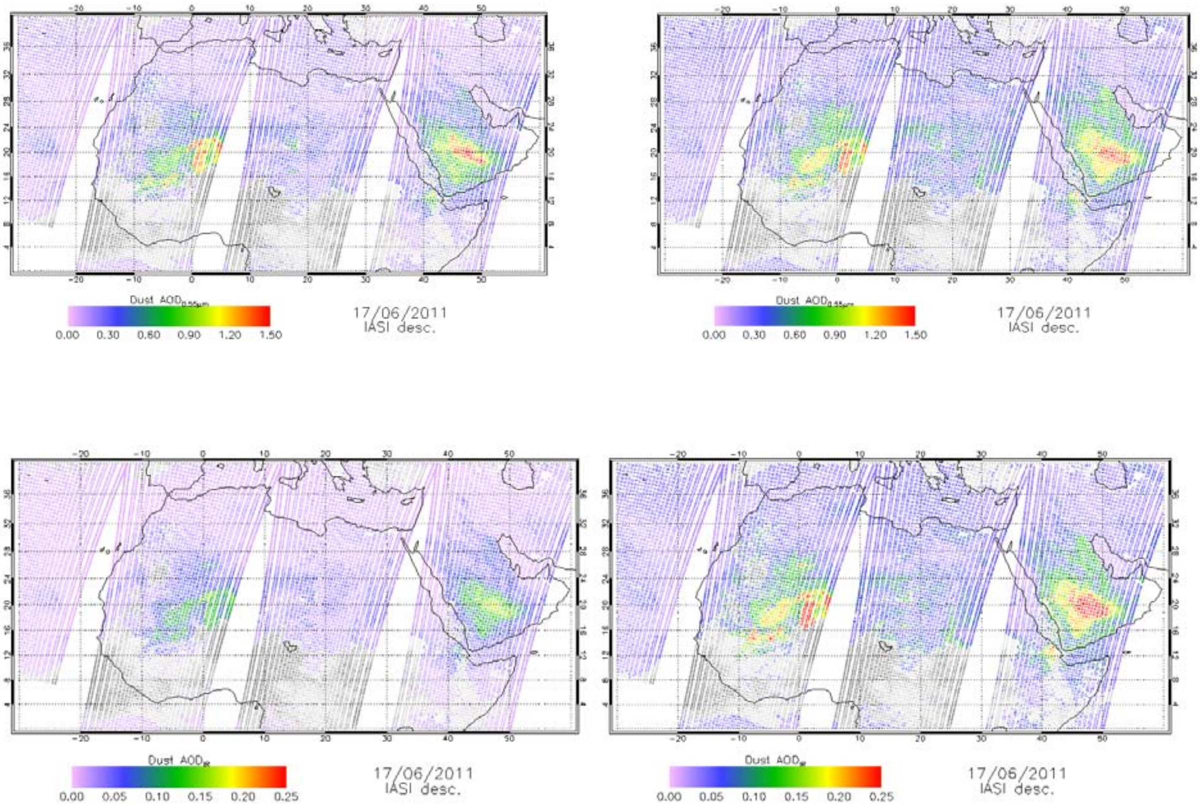

Figure 6: $AOD_{0.55\mu m}$ (top) and $AOD_{10\mu m}$ (bottom) for June 17th, 2011 over North Africa and Arabia as retrieved from IASI using FTIR (left) and Mie (right) dust spectra. The grey background represents the presence of ice clouds.

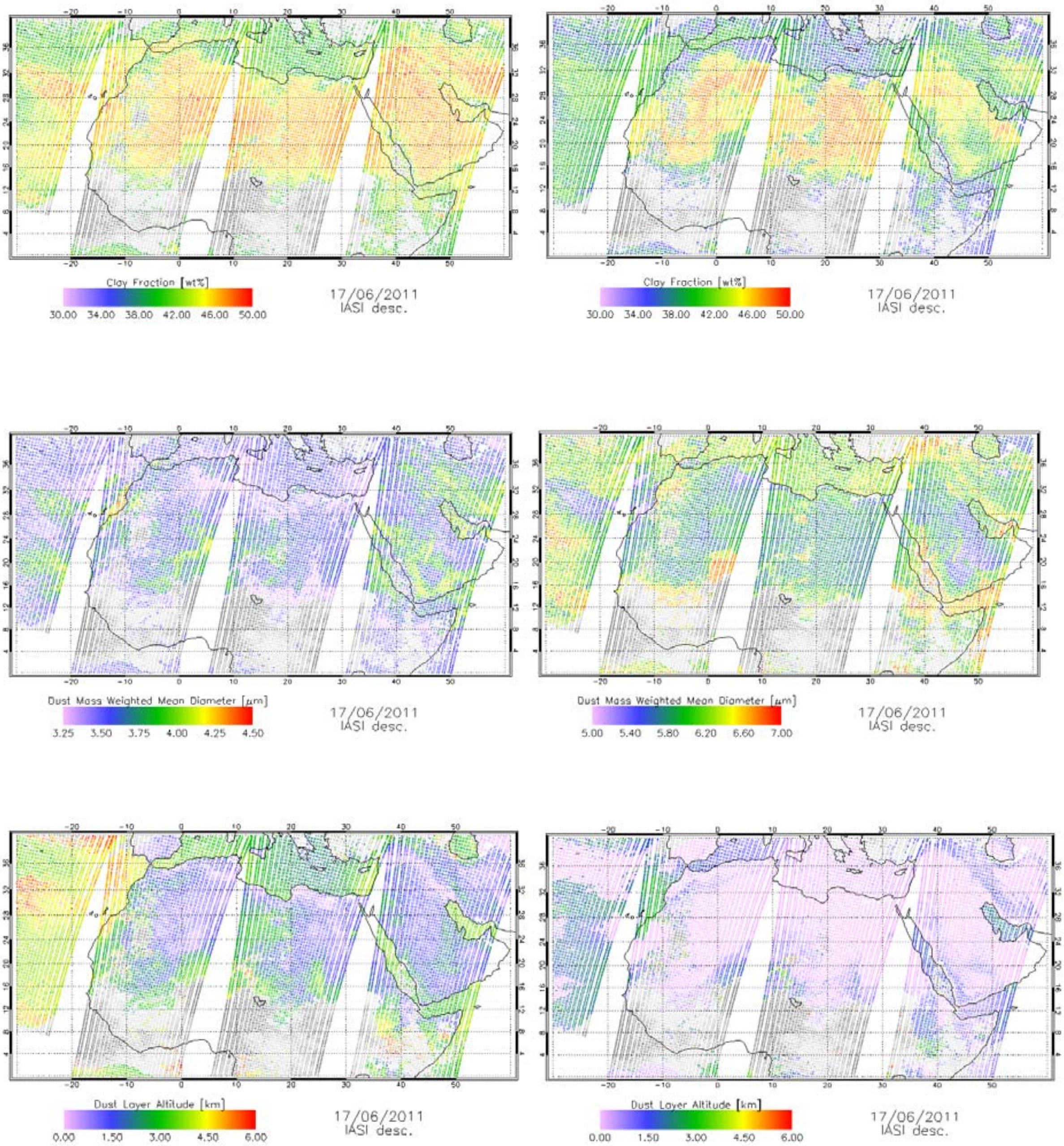

Figure 7: Clay (illite+kaolinite+montmorillonite) fraction (top), mass-weighted mean particle diameter (middle) and dust layer altitude (bottom) as retrieved from IASI with FTIR (left) and Mie (right) spectra for the Saharan and Arabian region on June 17th, 2011.

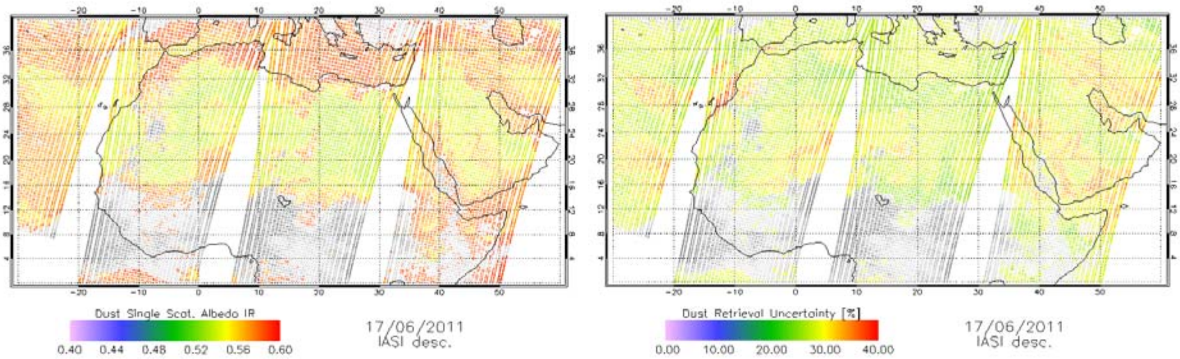

Figure 8: IR single scattering albedo (left) and AOD (at 0.55?) retrieval uncertainty (right) for the Mie version of the IASI retrieval for the Saharan and Arabian region on June 17th, 2011.

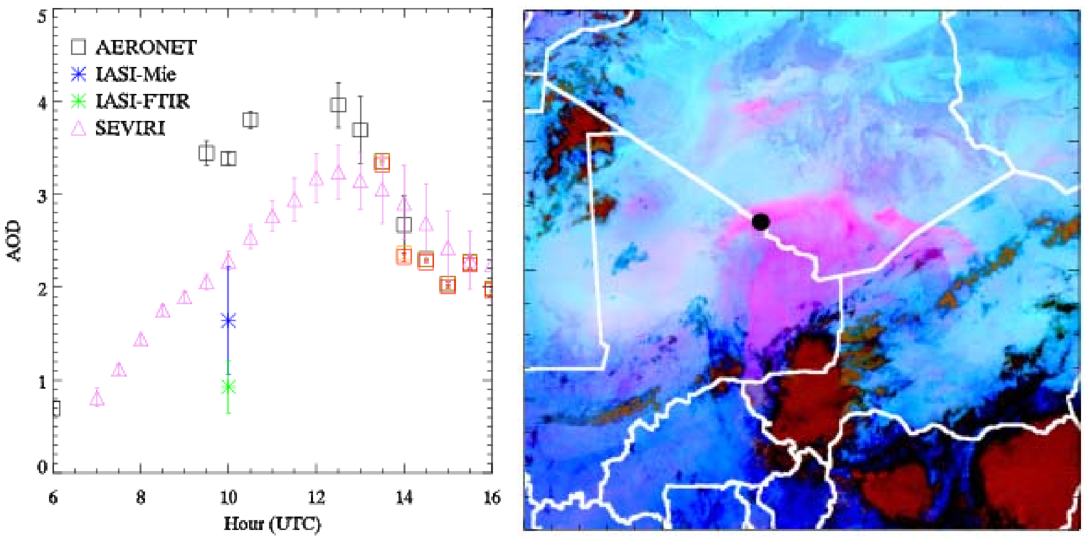

Figure 9: Dust activity over Bordj-Badji Mokhtar (BBM) on the 17th of June, 2011 updated from Fig. 10 in *Banks et al.* (2013). Left: time-series of AERONET and satellite retrieved AODs during the day (black squares are Level 1 AERONET, orange are Level 1.5, and red are Level 2); Right: RGB 'desert-dust' image from SEVIRI at 10:30 UTC (dust appears pink, thick clouds are red, and BBM is the black circle on the Algerian/Malian border). AERONET error bars are derived from the standard deviation of the mean of the measurements made within ±15min of each time slot, while satellite product error bars are derived from the standard deviation of the mean of the retrievals made within 25km of BBM.

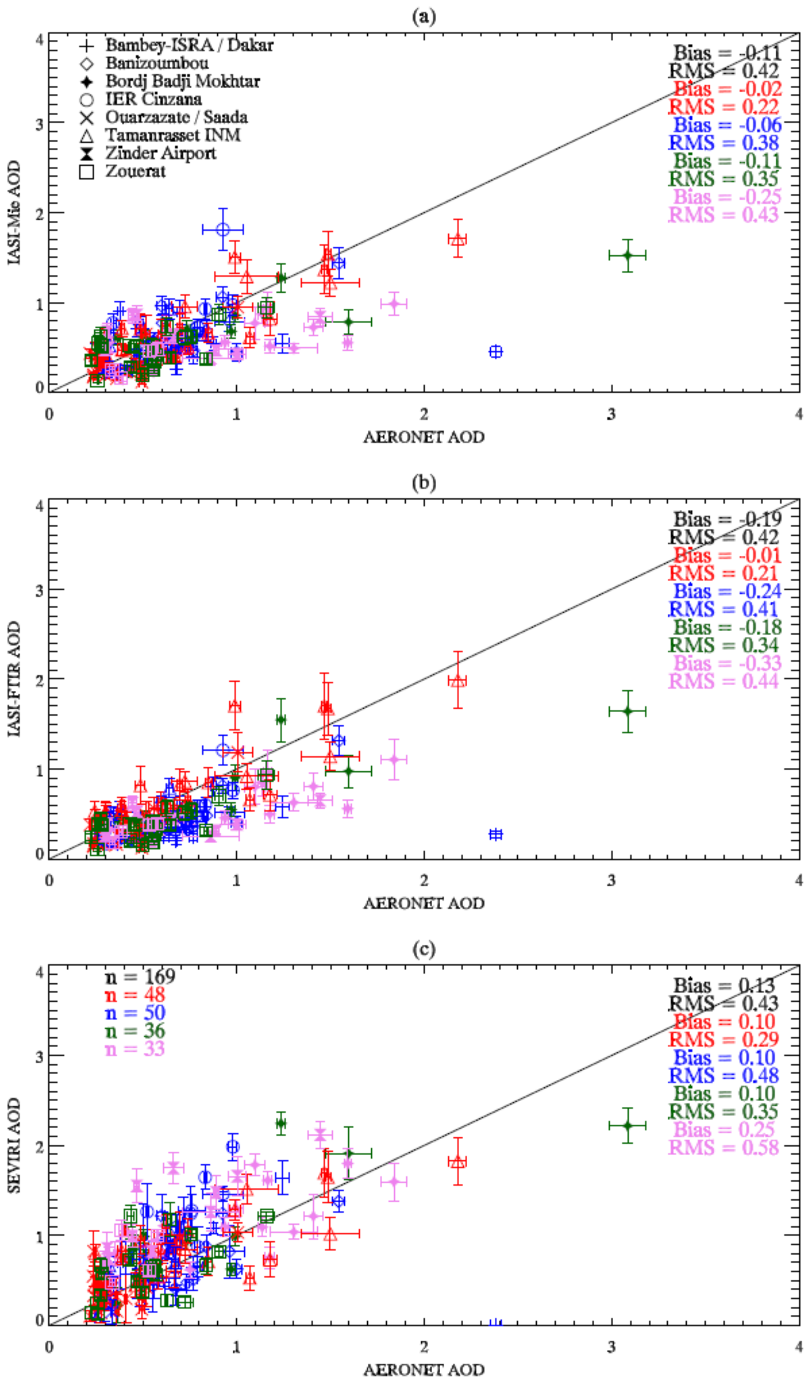

Figure 10: Scatterplots of Level 1.5 AERONET (total $AOD_{0.55\mu m}$) against satellite retrievals for June 2011 and June 2012: (a) IASI-Mie Dust $AOD_{0.55\mu m}$; (b) IASI-FTIR Dust $AOD_{0.55\mu m}$; (c) SEVIRI Dust $AOD_{0.55\mu m}$. Following Banks et al., 2013, individual sites are marked by varying shapes, and the different moisture and albedo regimes are marked as red (dry/dark), blue (moist/dark), green (dry/bright) and purple (moist/bright). The black symbols represent the overall statistics without subdivision by moisture or albedo. The albedo threshold is 0.3. The number of points (total and by regime) is identical for each panel, and is indicated in panel (c). For AERONET the error bars indicate the standard deviation of the mean of the measurements within three hours of the IASI

overpass, while for the satellite products the error bars represent the spatial standard deviation of the mean of the measurements within 25km of the AERONET sites for the relevant scene viewed.

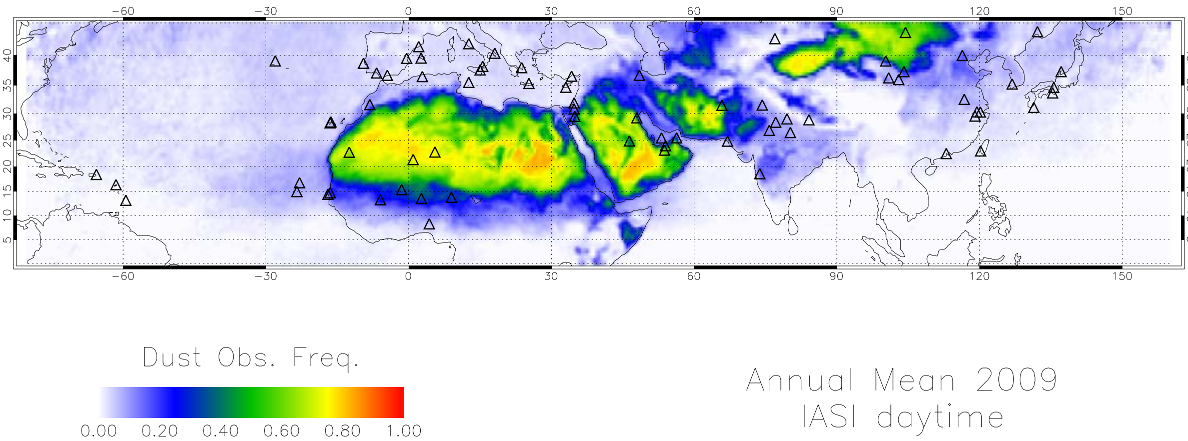

Figure 11: Frequency of dust retrievals for the year 2009 over the analysis domain. The black symbols indicate the locations of the AERONET stations used for evaluation.